

AD-A017 605

LASER WINDOW SURFACE FINISHING AND COATING SCIENCE

M. Braunstein, et al

Hughes Research Laboratories

Prepared for:

Air Force Cambridge Research Laboratories  
Defense Advanced Research Projects Agency

July 1975

DISTRIBUTED BY:

**NTIS**

National Technical Information Service  
U. S. DEPARTMENT OF COMMERCE

332062

AFCL-TR-75-0429

**LASER WINDOW SURFACE FINISHING  
AND COATING SCIENCE**

**M. Braunstein, S. D. Allen, A. I. Braunstein,  
C. R. Giuliano, R. R. Turk, V. Wang, D. Zuccaro**

**Hughes Research Laboratories  
3011 Malibu Canyon Road  
Malibu, California 90265**

July 1975

Semiannual Technical Report No. 1

Approved for public release; distribution unlimited

Sponsored by

Defense Advanced Research Projects Agency  
ARPA Order No. 2415

Monitored by

**AIR FORCE CAMBRIDGE RESEARCH LABORATORIES  
AIR FORCE SYSTEMS COMMAND  
UNITED STATES AIR FORCE  
HANSCOM AFB, MASSACHUSETTS 01731**

Reproduced by  
NATIONAL TECHNICAL  
INFORMATION SERVICE  
U.S. Department of Commerce  
Springfield, VA. 22151



ADA017605

UNCLASSIFIED

SECURITY CLASSIFICATION OF THIS PAGE (When Data Entered)

REPORT DOCUMENTATION PAGE		READ INSTRUCTIONS BEFORE COMPLETING FORM
1. REPORT NUMBER AFCL-TR-75-0429	2. GOVT ACCESSION NO.	3. RECIPIENT'S CATALOG NUMBER
4. TITLE (and Subtitle) LASER WINDOW SURFACE FINISHING AND COATING SCIENCE		5. TYPE OF REPORT & PERIOD COVERED Semiannual Tech Report 1 2 Dec 1974-2 June 1975
		6. PERFORMING ORG. REPORT NUMBER
7. AUTHOR(s) M. Braunstein, S.D. Allen, A.I. Braunstein, C.R. Giuliano, R.R. Turk, V. Wang, and D. Zuccaro		8. CONTRACT OR GRANT NUMBER(s) F19628-75-C-0135
9. PERFORMING ORGANIZATION NAME AND ADDRESS Hughes Research Laboratories 5011 Malibu Canyon Road Malibu, CA 90265		10. PROGRAM ELEMENT, PROJECT, TASK AREA & WORK UNIT NUMBERS 2415-n/a - n/a
11. CONTROLLING OFFICE NAME AND ADDRESS AF Cambridge Research Laboratories Hanscom AF Base, MA 01731 Contract Monitor: Dr. Harold Posen/LQO		12. REPORT DATE July 1975
14. MONITORING AGENCY NAME & ADDRESS (if different from Controlling Office)		13. NUMBER OF PAGES <del>67</del> 67
		15. SECURITY CLASS. (of this report) UNCLASSIFIED
		15a. DECLASSIFICATION/DOWNGRADING SCHEDULE
16. DISTRIBUTION STATEMENT (of this Report)  Approved for public release; distribution unlimited.		
17. DISTRIBUTION STATEMENT (of the abstract entered on Block 20, if different from Report)		
18. SUPPLEMENTARY NOTES This research was sponsored by the Defense Advanced Research Projects Agency, ARPA Order No. 2415.		
19. KEY WORDS (Continue on reverse side if necessary and identify by block number) Laser windows, Surface finishing, Thin films, Antireflection coatings, 10.6 $\mu\text{m}$ , 3.8 $\mu\text{m}$ , Laser damage studies, Surface characterization, Optical evaluation, 10.6 $\mu\text{m}$ ellipsometer, Potassium chloride, Zinc selenide, Doped and alloyed halides, Calcium fluoride		
20. ABSTRACT (Continue on reverse side if necessary and identify by block number) We report on the objectives and the progress achieved in a program to study the surface finishing and coating of laser windows for high energy laser applications in the 10.6 $\mu\text{m}$ , 5.3 $\mu\text{m}$ , and 3.8 $\mu\text{m}$ wave- length regions. The work on thorium tetrafluoride ( $\text{ThF}_4$ ) film prepar- ation under ultrahigh vacuum conditions has produced films having ab- sorption index values (K) in the range of 0.7 to $1.1 \times 10^{-3}$ . These values are the same as those we obtain using conventional high vacuum		

DD FORM 1473 1 JAN 73 EDITION OF 1 NOV 65 IS OBSOLETE

UNCLASSIFIED

SECURITY CLASSIFICATION OF THIS PAGE (When Data Entered)

UNCLASSIFIED

SECURITY CLASSIFICATION OF THIS PAGE (When Data Entered)

oil diffusion pumped systems. Surface finishing work for KCL placed emphasis on examination of various liquid etchants to determine their compatibility with pitch laps used for surface polishing. Ethanediol, glycerin, propanediol 1, 2, propanediol 1, 3, monoacetin, diacetin, and triacetin were found to have little or no dissolution action on pitch. Work on the development of a modulated light ellipsometer with operating capability at  $10.6 \mu\text{m}$  continued. Various feedback control stabilization schemes are described to provide stability to the light source and the zinc selenide photoelastic modulator used to obtain  $10.6 \mu\text{m}$  operation. Data on the refractive index of polycrystalline zinc selenide at  $10.6 \mu\text{m}$  as a function of angle are presented. The improvements made to our laser damage test facility are described. The range of pulse durations has been extended to cover from  $0.6 \mu\text{sec}$  to  $6 \mu\text{sec}$  and single longitudinal mode control consisting of a smooth temporal profile has been achieved.

UNCLASSIFIED

SECURITY CLASSIFICATION OF THIS PAGE (When Data Entered)

## TABLE OF CONTENTS

SECTION		PAGE
	LIST OF ILLUSTRATIONS . . . . .	5
I	INTRODUCTION. . . . .	7
II	TECHNICAL DISCUSSION. . . . .	11
	A. Surface Finishing . . . . .	11
	B. Coating Techniques. . . . .	20
	C. Optical Evaluation. . . . .	28
	D. Damage Studies . . . . .	42
III	SUMMARY . . . . .	65
IV	CONSULTATION AND VISITATIONS . . . . .	67
V	PRESENTATIONS . . . . .	69

## LIST OF ILLUSTRATIONS

FIGURE		PAGE
1	Etch rate for 7:1 acetic acid/HCl . . . . .	13
2	136x photomicrograph of etched KCl . . . . .	14
3	100x microcut (soft) . . . . .	19
4	100x standard SiC paper . . . . .	19
5	500x "soft" ground KCl, groove depth 1-1/2 $\mu\text{m}$ . . . . .	19
6	500x standard abraded KCl, groove depth 4 to 5 $\mu\text{m}$ . . . . .	19
7	Waveguide CO <sub>2</sub> laser . . . . .	29
8	ZnSe photoelastic modulator . . . . .	30
9	PbSnTe photovoltaic detector . . . . .	32
10	Calibration curve for double-driven ZnSe modulator . . . . .	34
11	Schematic of electronic components- infrared modulated light ellipsometer . . . . .	36
12	The three-component photoelastic modulator . . . . .	39
13	View of transverse discharge section with uv preionizers . . . . .	44
14	Simplified schematic of double discharge electrical pulse forming network . . . . .	45
15	Gas handling system for laser and sample chamber . . . . .	47
16	Laser damage facility . . . . .	48
17	Schematic of laser, optical cavity, optical train, alternators, detectors, alignment system, and sample chamber with microscope and focusing lens . . . . .	49

**Preceding page blank**

FIGURE		PAGE
18	Vacuum tight sample chamber with precision X,Y,Z translator, focusing lens, and microscope . . . . .	53
19	Sample position in sample chamber showing focusing lens and off-axis microscope objective . . . . .	53
20	Equivalent pulse length . . . . .	56
21	Preionizer and main discharge current for long pulse operation . . . . .	56
22	Equivalent pulse length . . . . .	57
23	Pulse slope measured with photon drag detector . . . . .	59
24	Single longitudinal mode pulse of 1 $\mu$ sec duration . . . . .	59
25	50 nsec/div expanded view of the main pulse . . . . .	59
26	(a) 4 $\mu$ sec equivalent pulse length, modified. (b) 6 $\mu$ sec single longitudinal mode pulse . . . . .	61

## I. INTRODUCTION

Hughes Research Laboratories (HRL) is engaged in a broad program to develop laser window surface finishing and coating technology. Extensive investigations are under way in many laboratories throughout the country, as well as at HRL to develop window materials that have both the low-optical absorption and the high tensile yield stress necessary to satisfy high energy laser system applications. Two classes of materials-the wide bandgap semiconductors and the alkali halides-have received major emphasis in these investigations. At present, serious limitations to window performance characteristics can exist because as the laser pulse duration is shortened and the peak power densities rise, the low damage threshold of the presently available coatings and surfaces can cause damage to occur below the bulk material damage threshold. This lowered damage threshold can be caused by the presence of pores and microcracks which can be present in window surfaces and coatings, and by the high optical absorption in the polished surfaces and coatings produced using presently available state-of-the-art surface finishing and coating techniques.

The goal of our program at HRL is to investigate the surface characteristics and the optical coatings applied to laser windows in order to develop optimized finishing and coating procedures so that the laser damage thresholds of the coatings and surfaces approximate as closely as possible the damage thresholds of the bulk window materials.

Our accomplishments in the initial phases of the program that we conducted in the period from 1 May 1973 to 31 October 1974 were reported in the final report, Contract AFCRL-TR-75-0041, entitled "Laser Window Surface Finishing and Coating Technology," January, 1975. We conducted a broad attack on some of the major problem areas in the surface finishing and coating of windows for use at the 10.6  $\mu\text{m}$   $\text{CO}_2$  laser wavelength. Early emphasis was placed on the ability to prepare reproducible surfaces on single crystal KCl and polycrystalline ZnSe (Raytheon CVD material) which were free of impurities and were

structurally representative of the bulk materials. Our success in this effort guaranteed that a "standard surface" was available for use in subsequent coating work which had as its goal the exploration of the potential of film preparation technologies other than sublimation or evaporation in conventional vacuum systems. These included deposition in ultrahigh vacuum, sputtering, physical vapor deposition, and chemical vapor deposition. Pulsed, 10.6  $\mu\text{m}$ , laser damage studies were conducted with the goal of determining the damage thresholds and elucidating the damage mechanisms of the window materials, both in the bulk and on the surface, and the coatings applied to them.

An important aspect of the program was the extensive chemical, physical, and optical characterization of surfaces and films. The effort had a twofold goal: first, to track progress and aid in the conduct of the work on the various tasks, and second, to assess the potential of the various instruments and techniques. The various surface physics tools used included electron microprobe analysis, Rutherford back-scattering of light ions, Auger electron spectroscopy, low energy electron diffraction, and scanning electron microscopy.

Carbon dioxide laser calorimetry to determine the 10.6  $\mu\text{m}$  absorption of films and surfaces was used extensively. Other standard optical evaluation methods used were infrared spectrophotometry, attenuated total reflection spectroscopy, and 10.6  $\mu\text{m}$  scattering and reflectance.

In addition a unique optical evaluation tool was designed in the form of a modulated light ellipsometer for use at 10.6  $\mu\text{m}$ . This instrument can be used for the precise determination of the optical constants of surfaces and films and is expected to be competitive with calorimetry for the determination of absorption coefficients for interfaces and films.

This report covers the work performed on our continuing program for the period 2 December 1974 to 2 June 1975. The objective of our research continues to be the development of surface finishing and coating technology for halide and semiconductor laser windows for use in high-power infrared laser systems. The window materials to

be investigated will include single and polycrystalline  $\text{KCl}$ ,  $\text{CaF}_2$ , doped and alloyed alkali halides and  $\text{ZnSe}$ . The principal laser wavelengths of interest are  $10.6 \mu\text{m}$ ,  $5.3 \mu\text{m}$ , and  $3.8 \mu\text{m}$ .

## II. TECHNICAL DISCUSSION

### A. Surface Finishing (R. R. Turk)

In our study of the chemical-mechanical etch-polishing of infrared laser window materials, we need to understand the mechanisms by which surface material is removed so we can produce infrared windows with undistorted surface structure. On potassium chloride (KCl) this type of surface absorbs less 10.6  $\mu\text{m}$  radiation and resists moisture. In addition, we must generate flat and parallel window surfaces to avoid beam distortion. Scratches and other surface artifacts must be minimized because they cause scattering and loss of beam power. Therefore, we have three objectives:

1. Produce windows with undistorted surface structure
2. Optically finished flat and parallel surfaces on these windows
3. minimize scratches and surface artifacts.

During this period we studied etchants for KCl, their removal rates and compatibility with optical lapping, and their use in chemical-mechanical polishing. Some work was also done on zinc selenide (ZnSe) and potassium bromide (KBr) surfaces.

#### 1. Absorptive Surface Layer

Previous studies<sup>1</sup> showed a drop in absorption of ten times for an optically-polished KCl crystal upon chemical polishing. This occurred in less than 15 sec immersion in concentrated HCl (12 normal) and before scratches were removed. However, optical figure was lost ( $\lambda/35 \rightarrow \lambda/18$  at 10.6  $\mu\text{m}$ ) after etching. We wish to find the thinnest layer, which must be removed for lowest absorption. This will guide us in chemical-mechanical polishing of KCl windows, and

---

<sup>1</sup> "Laser Window Surface Finishing and Coating Technology," Quarterly Status Report 2, Nov. 1973 to Jan. 1974, ARPA Order No. 2415, Code No. 3D10.

will give least loss of optical figure. To get this information, we need a slow-acting chemical polishing agent which will remove KCl in small increments, lowering absorption gradually. From measurements of thickness and absorption, minimum removal will be found for lowest absorption.

## 2. Slow Etch Development

For our first efforts, we used concentrated HCl as a primary etch-polish, modified by temperature changes, diluents and secondary etchants (see Table 1). Figure 1 is a typical graph of etch time versus amount removed for 7:1 acetic acid in HCl. (S. Allen's original curve for 12N HCl is included for comparison.) Removal rates are measured with a Dektak Profilometer, which records step height over the boundary between etched and masked areas (Fig. 2).

TABLE 1. Initial Etch-Rate Studies on Optically Polished KCl

Test Mixture, Conditions	Removal Rate, $\mu\text{m}/\text{min}$
HCl	7.0 to 10.0
HCl-Acetic Acid 1:7, 14°C	3.0 to 3.6
HCl-Acetic Acid 1:7, 25°C	3.4 to 4.4
HCl-Acetic Acid 1:7, 40°C	6.0 to 7.0
HCl-Acetic Acid 1:19	2.1 to 2.5
Acetic Acid	1.7 (rough surface)
HCl-Acetic Anhydride 1:2	2.9
HCl-Acetic Anhydride 1:2.5	2.0
HCl-Acetic Anhydride 1:7.5	1.1
HCl-Acetic Anhydride 1:15	0.8 (rough surface)
Acetic Anhydride	0
HCl-Triacetin 1:1	2.0 (rough surface)
Triacetin	0
HCl-isopropanol 1:1	2.0 (rough surface)
Isopropanol	0
Anhydrous HCl-isopropanol	0 (absorption unchanged)

T1749

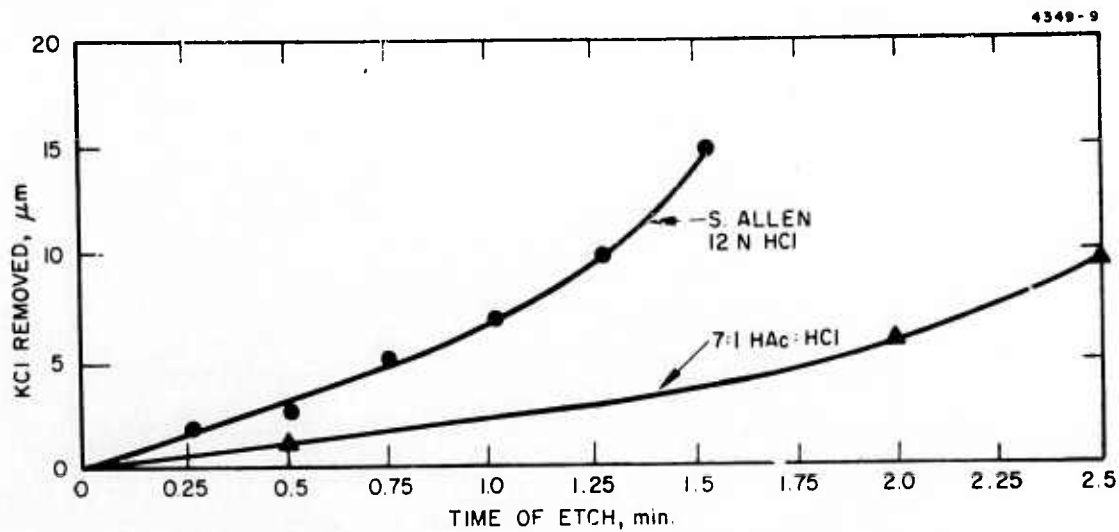
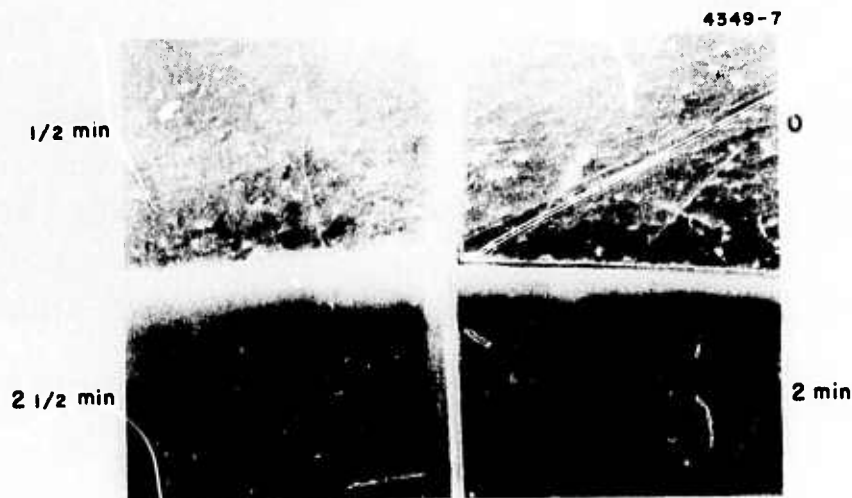


Fig. 1. Etch rate for 7:1 acetic acid/HCl.



<u>Quadrant</u>	<u>Time</u>	<u>Depth, <math>\mu\text{m}</math></u>
Upper Right	0 min	0
Upper Left	0.5 min	2.2
Lower Right	2.0 min	6.8
Lower Left	2.5 min	8.6

Fig. 2. 136 x photomicrograph of etched KCl showing areas with four different etching times.

From our work, we have learned the following:

1. Etch rates are lowered by dilution, but are only slightly lowered by temperature
2. Slower etchants (of this polar type) produce rough, unpolished surfaces
3. Acetic anhydride was most effective in reducing the etch rate of HCl with least loss of polishing action
4. Removal of surface  $\text{OH}^-$  ion alone did not lower absorption (anhydrous HCl in isopropanol).
3. Chemical Etches, Lap Compatibility

With chemical-mechanical polishing as our primary goal, we set thickness removal in abeyance and sought less hazardous and more effective slow etchants as polishing vehicles for optical finishing. First, we checked compatibility with optical pitch to find promising liquids (see Table 2). From this list, we chose etchants which dissolve KCl by chelating action in addition to polar solvent effects. Measured etch rates of these materials are listed in Table 3. We found that glycols and acetins offered a 30:1 range of etching rates. This choice of rates is important in chemical-mechanical finishing, where disturbed surface material must be removed as fast as it is formed, but etching must be slow enough to avoid losing optical figure after leaving the lap and before etchant is removed. Also, a slow etch might be used after optical finishing to remove extremely thin damage layers with no loss of figure.

#### 4. Chemical-Mechanical Polishing

As a preliminary test using ethanediol, we polished a piece of reactive atmosphere processed (RAP) KCl by chemical-mechanical means. We used Linde A abrasive in an etchant slurry on a lap of Politex Supreme, a soft, "poromeric" sponge-like material. Resulting calorimetric absorption was  $0.0003 \text{ cm}^{-1}$ , close to the minimum for this particular piece. This demonstrates that chemical-mechanical polishing is feasible, even though this piece was not flat

TABLE 2. Liquids Tested for Pitch Solubility  
(Microscopic Observation of Liquid on Fine Particles of Swiss Pitch)

Solvent	Soluble
Water	no
Glycerin	no
Monoacetin	no
Diacetin	no
Triacetin	no
Ethenediol	no-slight in 24 hours
Propanediol 1, 2	no-slight in 16 hours
Propanediol 1, 3	no-less in 16 hours
Tri-ethenediol	yes-slow
Methanol	yes
Ethanol	yes
Isopropanol	yes
Decanol	yes
Acetic acid, glacial	yes
Ammonium hydroxide (concentrated)	yes
Hydrogen peroxide (30%)	yes
Alkaline ferricyanide (diluted)	slight
Acetone	yes
Methylethyl ketone	yes
Trichloroethylene	yes
Carbon Tetrachloride	yes
Kerosene	yes
Toluene	yes
Freons	yes
Dimethylsulfoxide	yes
Dimethylformamide	yes
Tetra-hydro-furan	yes
Formic acid	yes
Ether	yes

TABLE 2. Liquids Tested for Pitch Solubility (Microscopic Observation of Liquid on Fine Particles of Swiss Pitch) (Contd)

Solvent	Soluble
Mineral Oil	slight
Optical immersion oil	slight
Dilute "Decontam" detergent	no
Concentrate "Decontam" detergent	yes

T1747

TABLE 3. KCl Etch Rates in Chelate-Type Solvents

Etchant	Removal Rate, $\mu\text{m}/\text{min}$
Ethanediol	3.3
Glycerin	1.5
Propanediol 1, 2	0.6
Propanediol 1, 3	0.3
Monoacetin	0.31
Diacetin	0.11
Triacetin	0

T1748

or polished under optical finishing conditions. We are now optically finishing KCl using etchants on pitch laps. Glycerin, ethanediol, and propanediol are being used, but some difficulty is found in etchant removal, as described below. Absorption measurements will be made when suitable flatness, parallelism, and cleanliness are attained.

##### 5. Surface Cleaning Problems

We clean the delicate surfaces of KCl after etching or polishing by an isopropanol rinse followed by vapor cleaning in Freon "TF." This treatment removes the non-etchant triacetin completely, as measured by calorimetric absorption. However, chelate-type

etchants used in chemical-mechanical polishing give problems in removal, since dilution by isopropanol causes a marked increase in etch rate. Ethanediol and propanediol both react with increased etch rate, while glycerin is too viscous to remove before deep etching occurs. This problem is being studied with emphasis on rapid uniform removal by spinning or ultrasonics, or by dilution with (nonaqueous) boric acid to stop etching action.

6. Scratches and Flatness

We are attempting to decrease scratches and maintain flatness by using softer laps (see Table 4). Total sphericity (flatness of both sides) is held to 2 or 3 fringes at 6328 Å and faces are parallel within 2 sec of arc. We are also changing from the non-etching triacetin to controlled etchants to remove highly-absorbing surface layers along with scratches.

TABLE 4. Optical Finishing of KCl

Sample	Lap <sup>a</sup>	Vehicle	Total Sphericity
A	Hard Pitch	Triacetin	3 fringes
1	Hard Pitch	Triacetin	2 fringes
2	Hard Pitch	Triacetin	2 fringes
3	Soft Pitch	Triacetin	2 fringes
4	Soft Pitch	Triacetin	5 fringes
5	Soft Pitch	Triacetin	2 fringes

<sup>a</sup>All windows cleaned/finished on flannel/abrasive lap.

T1750

7. "Soft" Grinding Paper

Windows must be ground flat and parallel before final pitch-polishing, and one of the final grit sizes is 600 (12 to 13 μm). This is very effective when used as a "fixed" abrasive (glued to paper,

Fig. 3), but damages delicate KCl surfaces deeply. We are experimenting with a "softer" 600-grit paper called "microcut" (Fig. 4) which leaves grooves and subsurface damage one-fourth as deep as those left by standard paper (Figs. 5 and 6). If flatness can be maintained and scratches minimized, this low-damage preparatory step should reduce time needed for final polishing and etching, with lower residual absorption.

#### 8. Alternate Lap Material

Porous vycor glass is being examined as a possible alternate lap for optical pitch. Insoluble in most liquids and hard enough to maintain a flat surface, it also has 28% interconnected porosity of 40 Å size. Thus, it can serve as a liquid reservoir and also provide "anchoring" sites for fine abrasive. However, it has proved difficult to handle, being sensitive to strains of fabrication and liquid absorption.

#### 9. Alternate Surface Treatments

Damaged surface layers on KCl will form grains of undamaged material at room temperature or slightly above, because KCl has a low recrystallization temperature (atomic re-ordering). Heat lamp treatment is used in our work to achieve moisture resistance of surfaces after finishing, and may be used to lower absorption in the future, since both phenomena depend upon reduction of distorted structure.

We are studying surface removal by chemical reaction, using silver nitrate solution on KCl. Silver chloride is repeatedly formed and removed by polishing, giving a uniform etch-effect. However, it is difficult to finally remove the last traces of silver chloride without damaging the KCl surface.

#### 10. New ZnSe Etchant

Zinc selenide may now be chemically-mechanically polished using an aqueous mixture of ammonium hydroxide and hydrogen

600 grit paper comparisons

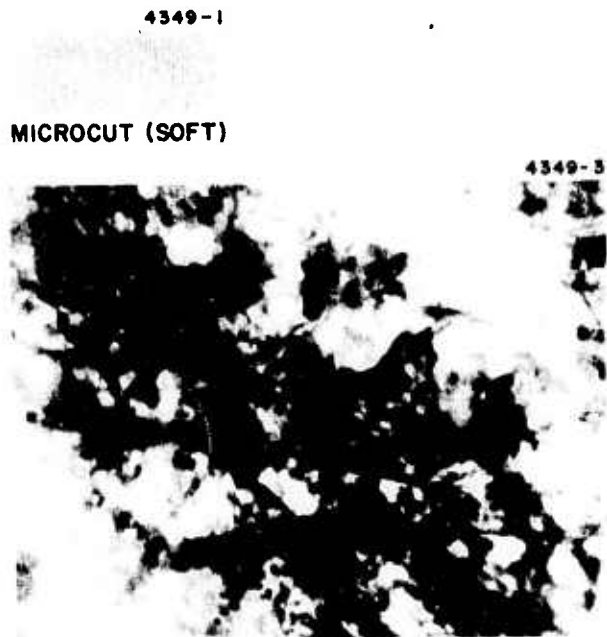


Fig. 3. 100x microcut (soft).

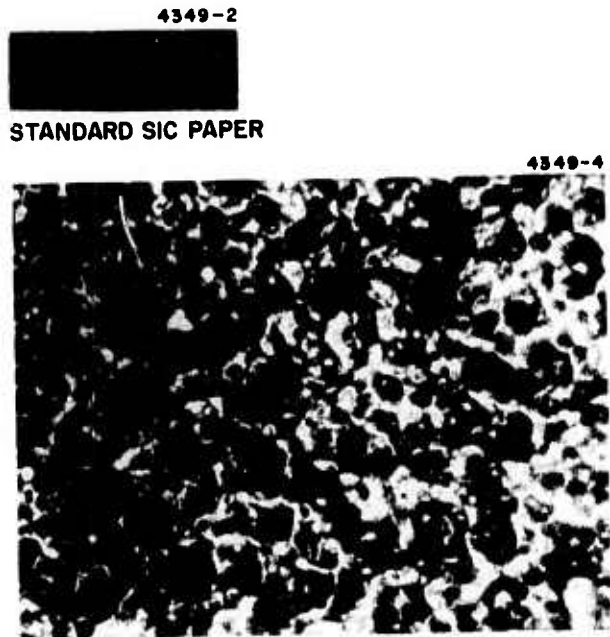


Fig. 4. 100x standard SiC paper.



Fig. 5. 500x "soft" ground KCl, groove depth 1-1/2  $\mu\text{m}$ .

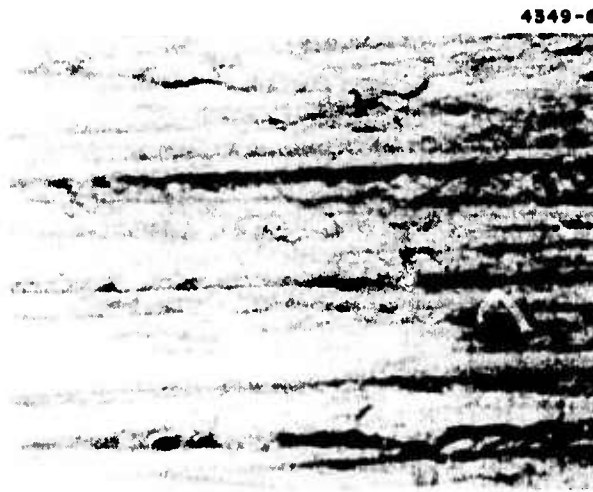


Fig. 6. 500x standard abraded KCl, groove depth 4 to 5  $\mu\text{m}$ .

Note: Lower density of abrasive particles in "soft" paper, smaller abraded grooves in KCl.

peroxide. This solution, in the proportions of 1:1:18 water, leaves an undamaged surface after optical finishing. It has the advantage over our previous etchant (alkaline potassium ferricyanide) because it does not leave hard crystals which cause scratches while drying on the optical lap.

#### 11. Chemical Polish for Potassium Bromide

Hydrobromic acid is being used to chemically-polish potassium bromide. Scratch-free, low-absorption surfaces are obtained that are similar to those on KCl after HCl treatments. Measured calorimetric absorption after a 20-sec etch was  $0.0002 \text{ cm}^{-1}$ , but moisture resistance was not as marked as for etched KCl.

#### 12. Finishing Summary

We are polishing KCl optically flat and parallel by chemical-mechanical methods using etchants with known etching rates which do not dissolve optical pitch. Comparative etch rates, pitch solubility, and mode of KCl attack are being investigated with reference to the multiple objectives of flatness, parallelism, low absorption, and freedom from scratches. We are testing a low-damage grinding technique, and are considering alternate ways of relieving or removing the damaged surface layers that give high absorption. Zinc selenide is now being prepared using an improved etchant for optical chemical-mechanical polishing.

#### B. Coating Techniques (D. Zuccaro)

During the course of our program it is our objective to prepare antireflection (AR) film coatings for candidate infrared laser window materials by three film preparation techniques: evaporation in high and ultrahigh vacuum (UHV), ion beam sputtering, and chemical vapor deposition. Using these preparation techniques the films are compared in an effort to determine an optimized method of preparation for use of the films in high energy laser window applications.

## 1. Ultrahigh Vacuum Film Deposition

During this period the program has two major objectives. The first is to complete the evaluation of single component optical films deposited under UHV conditions. The specific questions being considered are (1) "Are there significant differences between films deposited in UHV systems and conventional oil pumped vacuum systems?" (2) "Are there any significant differences in the  $\text{ThF}_4$  films obtained using optical materials prepared by different processes and obtained from different sources?" (3) "What is the optimum substrate surface temperature?" and (4) "Are there any effects on optical film properties associated with the background residual gases in the vacuum system?" The second major objective is to deposit two component antireflection coatings under UHV conditions and to compare these films with those prepared under ordinary vacuum conditions.

a. Experimental Results — The study of vapor deposited  $\text{ThF}_4$  films on KCl and ZnSe substrates under UHV conditions was completed during this report period. The KCl substrates were polished and coated with carbolene to protect the surfaces until the time of use. Potassium chloride surfaces were etched in concentrated HCl, using procedures developed previously,<sup>1</sup> just prior to being loaded into the vacuum systems and the ZnSe substrates were used in the as polished condition. The  $\text{ThF}_4$  evaporation material included single and polycrystalline reactive atmosphere processed (RAP) material produced at the Hughes Research Laboratories and polycrystalline  $\text{ThF}_4$  produced by Cerac (type TS 108).

An all-metal ultrahigh vacuum system used for film preparation was rough pumped by means of a gas aspirator pump and zeolite sorption pumps. The system uses an ion pump and a titanium sublimation pump to maintain ultrahigh vacuum conditions. The system was baked at  $225^\circ\text{C}$  for 30 or more hours. Substrates were maintained at a

---

<sup>1</sup>Ibid.

temperature of about 50 to 100°C greater than the rest of the system during the evacuation and bake out. Residual gas analysis and the evaluation of outgassing during depositions was performed with a Finnigan Quad 400 quadrupole mass analyzer.

The optical films were deposited over half of the surface of 4 cm diameter substrate samples. After removal from the system, the absorption of the coated and uncoated portions of the surfaces were determined by laser calorimetry. Film thicknesses were measured by Sloan Dektak and Car Zeiss interferometers.

The optimum substrate temperature during deposition was found to be in the range of 150 to 200°C. Deposition on surfaces at lower temperature produced films which had distinct absorption bands at 2.8  $\mu\text{m}$  and 6.1  $\mu\text{m}$  associated with water bands. Deposition at higher temperatures produced  $\text{ThF}_4$  films on KCl which tended to crack and flake off. The thermal stress problem did not appear to be as severe for the ZnSe substrates.

The  $\text{ThF}_4$  films prepared exhibited k values in a range from 0.7 to  $1.1 \times 10^{-3}$ . Several samples of  $\text{ThF}_4$  films that had k values outside this range were deposited on KCl substrates that had abnormally high absorption values. These we attributed to an imperfect surface etching operation. As a consequence, an additional inspection of the etched surface against a black background with low angle illumination was added to our procedures to detect such fogged surfaces. When this procedure was used, the films produced had consistently lower k values. The absorption index (k) values we obtain using ultrahigh vacuum are in the same range as those we get using conventional high vacuum oil diffusion pumped systems.

An electron microprobe analysis was made on two  $\text{ThF}_4$  films deposited on KCl to determine if any other metals were present in the films. The analysis showed only thorium and fluorine to be present in significant concentration. A trace amount of carbon was detected, but this is not significant as it is easily picked up on surfaces in the calorimetry and thickness measurement operations.

A quadrupole mass spectrometer was used to analyze the residual gases present in the vacuum system and those evolved during the vapor deposition process. The goal was to determine if there was any significant differences in the optical quality of films that could be associated with the presence of specific background gases or specific impurities in the  $\text{ThF}_4$  starting materials.

Before the bakeout of the system, the principal gases in the system were  $\text{N}_2$  and  $\text{H}_2\text{O}$ . After bakeout, the partial pressure of water was generally less than 1% of the major constituent which is fluorine. This means that the water vapor pressure in the system was on the order of  $10^{-11}$  Torr. The partial pressure of water can increase during the deposition of  $\text{ThF}_4$  as a result of the release of water from the  $\text{ThF}_4$ . It was discovered that significantly less water was evolved from the single crystal  $\text{ThF}_4$  grown by the RAP method as compared with the optical grade material that is formed into 1/8 in. lumps. This can be seen in the relative magnitudes of the 18 amu peak in Tables 5 and 6.

Two different sources of  $\text{ThF}_4$  materials were analyzed and found to exhibit different outgassing characteristics. The results of the study of the outgassing of single crystal RAP-grown  $\text{ThF}_4$  are shown in Table 5. Columns 1 through 7 are mass spectra taken during successive stages of heating of the  $\text{ThF}_4$  crystal. The mass spectra in columns 8, 9, and 10 were taken during the deposition of the  $\text{ThF}_4$ .

At the lowest temperature (column 1, Table 5), the major gases evolved from the crystal are  $\text{H}_2$ ,  $\text{CH}_4$ ,  $\text{C}_2\text{H}_4$ , and  $\text{CO}_2$ . These gases are believed to result from surface adsorption of methanol and acetone during the optical polishing of the surface. At higher temperatures, He (a carrier gas used in the RAP operation) is evolved (columns 3 and 4). The evolution of a significant amount of CO also occurs at a higher temperature (column 4). The CO is believed to have formed during the RAP operation as a result of the reaction of a small concentration of oxygen containing gas with the graphite walls of the reaction chamber. At that temperature and higher temperatures, a

TABLE 5. Mass Spectra Taken in Run 23 Before and During the Vapor Deposition of ThF<sub>4</sub>\*

	1	2	3	4	5	6	7	8	9	10
Total Pressure, Torr	$8 \times 10^{-8}$	$6.5 \times 10^{-8}$	$8.5 \times 10^{-8}$	$2 \times 10^{-7}$	$1.5 \times 10^{-7}$	$2 \times 10^{-7}$	$3 \times 10^{-7}$	$3 \times 10^{-7}$	$3 \times 10^{-7}$	$2.8 \times 10^{-7}$
Atomic Mass										
2	250	50	6	6	5	10	10	7	7	10
4	5	90	120	110	80	70	70	60	42	50
12	10			20	2					
14	30			1	1	1				1
15	160	5	2	1	1	1	5	2	3	6
16	190	8	2	10	5	2	4	5	4	9
18	20	5	1							
19	50	42	55	70	92	152	260	990	860	250
20	50	10	6	10	18	75	80	50	50	55
26	20									
27	50	4								
28	110	90	80	530	140	77	68	38	52	40
29	35			10	1					
33				10	12	15	5			
39	12	.5								
40	3	1				8	5			1
41	20	.5								
42	7	.5				3				
43	15	.3				2				
44	70	4		12	2		2			4
47		2		11	17	20	4			
66				5	5					
85		62	120	250	510	540	150	40	20	15
86				10	22	22	6			
87				5	17	16	4			

\* Mass spectra taken in Run 23 before and during the vapor deposition of ThF<sub>4</sub> (single crystal sample K62 C) onto KCl substrates. Data in Columns 1 through 6 taken while outgassing the ThF<sub>4</sub>, column 7 taken just before deposition, columns 8, 9, and 10 taken at the 1/4, 1/2, and 3/4 point in the deposition.

TABLE 6. Mass Spectra Taken in Run 25 Before, During, and After the Deposition of  $\text{ThF}_4$ \*

	1	2	3	4	5	6	7
Total Pressure, Torr	$2 \times 10^{-9}$	$3 \times 10^{-9}$	$6 \times 10^{-8}$	$8 \times 10^{-8}$	$1.2 \times 10^{-7}$	$2 \times 10^{-7}$	$1 \times 10^{-8}$
Atomic Mass							
2	4	10	44	1500	30		4
4	3	2	20	44	7		20
12		4	20	62	35	12	1.5
14	3	15	125	50	70	54	5
15	6	88	340	120	100	50	24
16	10	115	350	200	160	68	50
17	5	9	18	19	10	6	3
18	10	12	48	35	30	25	3
19	500	900	1150	1700	1450	3200	1350
20	25	40	140	100	125	290	51
22	1	1	8	5	7	5	3.5
26	1	6	30	12	8	5	4
27	2	10	60	22	14	8	5
28	60	70	400	1950	2100	900	80
29	1.5	9	28	30	28	12	5
30	1	4	8	8	7	3.5	3.5
33			1.5	8	6	2.5	
35	1.5	1.5	2	2	3	2	1.5
37		1.5	4	2.5	2	2	1
39		4	14	8	5	4	2
40	3.5	6	13	20	94	28	10
41		5	18	10	6	4	2
42		3	8	6	4	2.5	1.5
43		3	7	4	4	2.5	2
44	2.5	12	100	80	70	16	2
47			3	9	6	2	
55		2	4	3			
56		2	3.5	3			
64		1	2	2	7	2	
66			2	3	6	2	
67			2	2.5	2.5		
68			1.5	1.5	3.5		
78			3	2.5			
81				7			
85			14	140	210	7	
86			1.5	8	10		
87			1.5	4.5	6		

\* Mass spectra taken in Run 25 before, during and after the deposition of  $\text{ThF}_4$  (Cerac TS108-1/8 in. lump size) on to KCl substrates. Data in column 1 taken before heating the source, in columns 2 through 5 during the outgassing of the source, in column 6 during the deposition and in column 7 taken 2 hours after the deposition.

significant amount of  $\text{SiF}_4$  is evolved (columns 4, 5, and 6). Although this material could have formed by the chemical attack of silicon impurity in the graphite chamber walls, it is probably the consequence of silicon impurity in the thorium materials. After the evolution of these gases is completed, a shutter is removed and the film is deposited.

The outgassing characteristics of optical grade  $\text{ThF}_4$  (1/8 in. lump size) is shown in Table 6. The first column gives the mass spectra of the residual gas present before heating the  $\text{ThF}_4$  source. Columns 2 through 5 are mass spectra taken during the heating of the source, 6 was taken during the  $\text{ThF}_4$  deposition, and 7 was taken 2 hours later. The first compounds released are  $\text{CO}$ ,  $\text{CH}_4$ ,  $\text{CO}_2$  and  $\text{H}_2\text{O}$  (column 3). At a higher temperature  $\text{H}_2$ ,  $\text{CO}$ , and  $\text{SiF}_4$  are the major species released by the  $\text{ThF}_4$ .

It was not possible to determine if the differences in the  $\text{ThF}_4$  materials resulted in differences in the  $\text{ThF}_4$  films, because of the experimental uncertainty in the measured  $k$  values. These are associated with variations in the substrate surfaces and in the measurement techniques. This question deserves more attention when the processing of substrate materials is advanced to produce uniform surfaces.

A second part of our effort was to deposit multilayer anti-reflection coatings on ZnSe and KCl under UHV conditions. The coating designs were determined under Contract F33615-73-C-5044 for the Air Force Materials Laboratory. The coatings used ZnSe and  $\text{ThF}_4$  on KCl with optical thicknesses of 0.041 and 0.322  $\lambda$ , respectively and  $\text{ThF}_4$  and ZnSe on ZnSe with optical thicknesses of 0.132 and 0.052  $\lambda$ , respectively. A problem occurred when KCl substrates (coated on one side) were returned to the vacuum station for a deposition on the other surface. The original coating on the KCl substrate cracked and peeled during the bakeout process. The films on the ZnSe substrates were not sensitive to thermal stress cracking.

A new sample mounting technique is being developed to eliminate the KCl film coating problem. The substrates will be mounted in a flange ring which can be flipped to permit deposition on both surfaces during a single evacuation operation. The new design will permit the deposition of two component coatings on both surfaces of four individual samples. Glow discharge will be used to clean the surfaces. A transmission type optical monitor system will be used to monitor the film thickness during deposition.

## 2. High Vacuum Film Desposition

In our studies on the surface finishing and antireflective coatings for alkali halides for 10.6  $\mu\text{m}$  applications our objective has been to prepare antireflective coatings for KCl with both absorption and reflection losses less than 0.1% per surface. We have not been able to achieve this objective with two-layer film coatings because of the high optical absorption in the low index  $\text{ThF}_4$  film used in the coating design. Recently we have considered the use of three-layer antireflective coatings in which the  $\text{ThF}_4$  thickness can be reduced, thereby minimizing the optical absorption.

Two coating designs consisting of  $\text{As}_2\text{S}_3/\text{ThF}_4/\text{As}_2\text{S}_3$  and  $\text{As}_2\text{S}_3/\text{KCl}/\text{As}_2\text{S}_3$  theoretically meet our program goal requirements. Preliminary experimental results show that the three-layer coating designs on KCl substrates show promise of meeting our goals.

a. Experimental Results - The reduction to practice of the  $\text{As}_2\text{S}_3/\text{ThF}_4/\text{As}_2\text{S}_3$  three layer coating design, in preliminary experiments, resulted in 10.6  $\mu\text{m}$  absorption and reflection values of 0.1% and 0.7% per surface, respectively. The high reflectance value can easily be lowered with fine tuning the optical thickness of the coatings.

The three-layer design,  $\text{As}_2\text{S}_3/\text{KCl}/\text{As}_2\text{S}_3$ , on single crystal KCl substrates resulted in absorption and reflectance values of 0.09 and 0.06% per surface, respectively. Although this design meets the goal of less than 0.1% loss, continued emphasis will be placed on the coating deposition process work in efforts to minimize optical surface losses even further.

### C. Optical Evaluation

#### 1. Infrared Modulated Light Ellipsometer (S. D. Allen and A. I. Braunstein)

The 10.6  $\mu\text{m}$  modulated light ellipsometer has been described in detail elsewhere,<sup>2,3</sup> and only a brief description of the unique components will be included here. The optical train consists of light source, polarizer, photoelastic modulator, sample, analyzer, and detector.

The light source is a waveguide  $\text{CO}_2$  laser (Fig. 7) capable of emitting one watt cw  $\text{TEM}_{00}$  output. For our purposes, a lower intensity (several hundred milliwatts), achieved by lowering the gas pressure, is sufficient. The polarizer and analyzer are gold wire grids on antireflection coated ZnSe. The waveguide  $\text{CO}_2$  laser is polarized by an intracavity grating and therefore the polarizer is for alignment correction purposes only. The photoelastic modulator (PEM) is essentially a dynamic variable quarter wave plate in which the maximum retardation can be set to correspond to  $\lambda/4$  or other desired retardation at the wavelength of interest. For IR operation the PEM is a double driven, resonantly operated ZnSe bar AR coated for operation at 10.6  $\mu\text{m}$  (Fig. 8). For a 1/2 in. thickness of ZnSe  $\lambda/4$  maximum retardation can be achieved beyond the transparency limit of the material without exceeding the elastic limit of ZnSe. The detector is a PbSnTe photovoltaic device with a 0.5 mm by 0.5 mm surface area and a ZnSe window (Fig. 9).

---

<sup>2</sup>S. D. Allen, A. I. Braunstein, M. Braunstein, J. C. Cheng, and L. A. Nafie, "Modulated Light Ellipsometer for Ultraviolet, Visible, and Infrared Measurements of Thin Films and Surfaces," presented at the 1974 IR Window Materials Conference, Tucson, Arizona.

<sup>3</sup>S. D. Allen, A. I. Braunstein, M. Braunstein, J. C. Cheng, and L. A. Nafie, "A 10.6 Micron Modulated Light Ellipsometer," presented at the International Conference on Optical Properties of Highly Transparent Solids, Waterville Valley, New Hampshire.

M10733

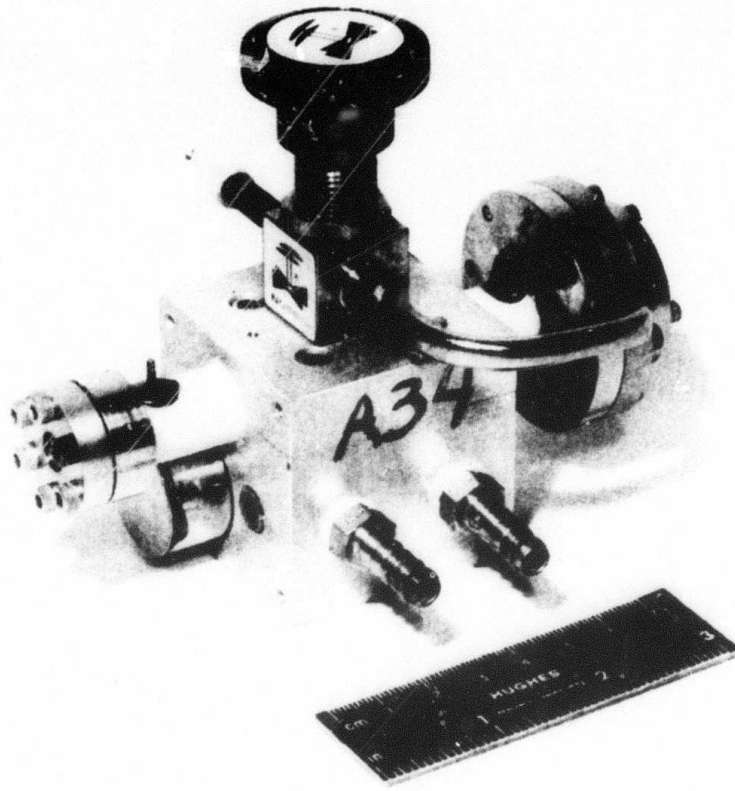


Fig. 7. Waveguide CO<sub>2</sub> laser.

M10735

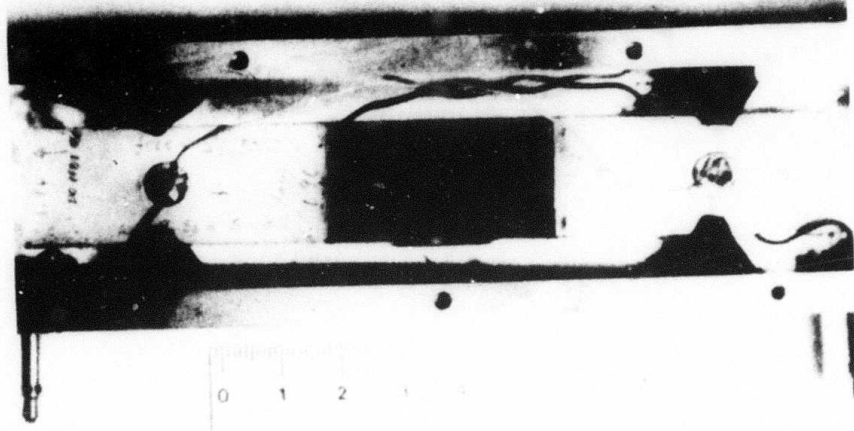


Fig. 8. ZnSe photoelastic modulator.

M10734

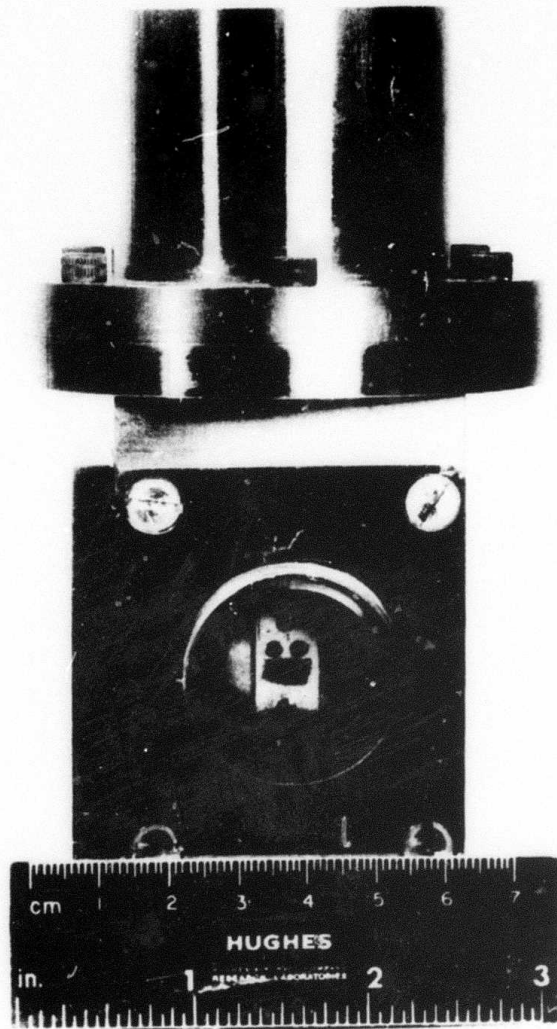


Fig. 9. PbSnTe photovoltaic detector.

The ellipsometric parameters are extracted from the signal received by the detector by taking ratios of the signals at the modulator resonance frequency,  $\omega$ , the second harmonic  $2\omega$ , and the "DC" signal which is actually chopped at a low frequency ( $10^2$  Hz). The resonance frequency,  $\omega$ , of modulator elements of the size used is approximately 50 kHz. The equations for a modulation amplitude where  $J_0(2.405) = 0$ , are given below:

$$\frac{I_{2\omega}}{I_{DC}} = -4J_2(2.405) \frac{r_{\parallel}/r_{\perp}}{1 + (r_{\parallel}/r_{\perp})^2} \cos \Delta \cos 2\omega t \quad (1)$$

$$\frac{I_{\omega}}{I_{DC}} = 4J_1(2.405) \frac{r_{\parallel}/r_{\perp}}{1 + (r_{\parallel}/r_{\perp})^2} \sin \Delta \sin \omega t \quad (2)$$

$$\frac{I_{\omega}}{I_{2\omega}} = -\frac{J_1(2.405) \sin \omega t}{J_2(2.405) \cos 2\omega t} \tan \Delta \quad (3)$$

$r_{\parallel}, r_{\perp}$  = amplitudes of reflection coefficients for  $\parallel$  and  $\perp$  polarization

$\Delta$  = phase difference between  $\parallel$  and  $\perp$  polarizations on reflection

$\phi$  (retardation angle) =  $\phi_m \sin \omega t$

$\omega$  = frequency of modulator.

$$\tan \psi = r_{\parallel}/r_{\perp}.$$

## 2. Problems and Proposed Solutions

An initial problem is one of calibration of the modulator, i. e., determining the functional dependence of  $\phi_m$ , the amplitude of the phase, on the applied voltage.

$$\phi_m = P \frac{2\pi d}{\lambda} V Q, \quad (4)$$

where

$d$  = thickness of the modulator

$V$  = voltage applied to quartz transducers

$Q$  = quality factor of the whole modulator

$\lambda$  = wavelength of the measurement

$P$  = proportionality factor containing the stress optic coefficient of ZnSe and the piezoelectric constant of quartz.

It has been shown that for the drive voltages of interest the  $Q$  of the system remains constant with changes in  $V$  (assuming no temperature change), so that  $\phi_m = P'V$ , where  $P'$  is a new proportionality constant for a particular modulator. For a fixed wavelength,  $P'$  can be determined by plotting  $I_{DC}$  or  $I_{2\omega}$  versus applied voltage, e. g.,  $I_{DC} = 1/4(1 - J_o(\phi_m))$  with no sample. At short wavelengths (He-Ne laser at  $0.6328 \mu\text{m}$ ) the condition  $J_o(\phi_m) = 0$  is reached several times before the maximum attainable  $V$ . Calibration is thus accomplished relatively easily by curve fitting. For  $10.6 \mu\text{m}$ , however,  $\phi_m$  is relatively small, even at the maximum voltage, and direct curve fitting is very difficult for either  $I_{DC}$  or  $I_{2\omega}$ .

For the normal optical system (polarizer at  $-45^\circ$  crossed with the analyzer at  $+45^\circ$ )  $I_{DC} = 1/4(1 - J_o(\phi_m))$ . If the polarizer is set at  $+45^\circ$  or parallel with the analyzer,  $I'_{DC} = 1/4(1 + J_o(\phi_m))$ . We can then measure the quantity

$$A(V) = \frac{I_{DC}}{I'_{DC}} = \frac{1 - J_o(\phi_m)}{1 + J_o(\phi_m)} \quad (5)$$

and solve for  $J_o(\phi_m)$ . A  $10.6 \mu\text{m}$  calibration curve for the double driven ZnSe modulator is given in Fig. 10.

If the ZnSe modulator bar is not antireflection coated, its use and calibration become difficult. For  $10.6 \mu\text{m}$  the faces of the modulator bar are parallel enough to act as an etalon; i. e., for the coherent

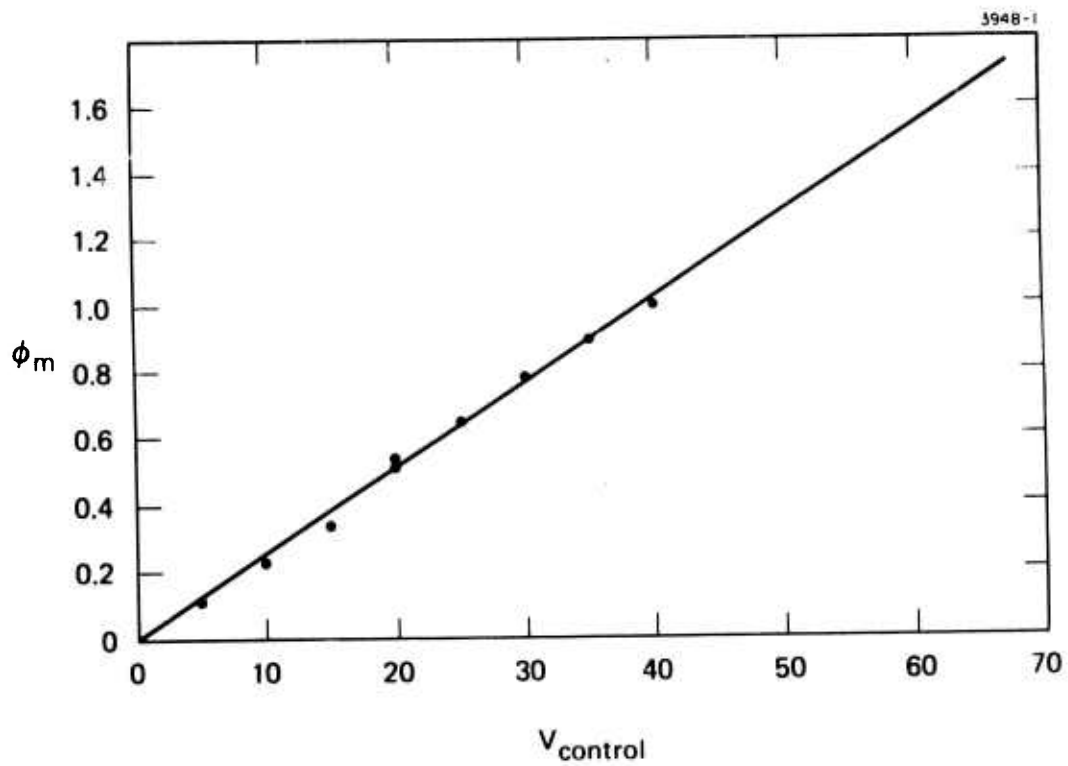


Fig. 10. Calibration curve for double driven ZnSe modulator. Control is a DC proportional to the peak-to-peak voltage applied to the quartz transducers.

radiation of the laser, the modulator can be a resonant cavity if the thickness is an integral number of half wavelengths. Experimentally, the modulator draws a small amount of power, and as it heats up and expands, it tunes in and out of resonance. In addition to the etalon effect, the temperature variation of the modulator ensemble (drivers and optical element) changes the Q and/or the resonant frequency of the device. Therefore, for a given drive voltage,  $V_c$ , the retardation amplitude may change with time. This effect, although of significantly lower magnitude than the etalon effect, is most apparent at high drive voltages and will affect the accuracy of the measurements.

Another source of instability in the system is the light source. Variation of the "DC" level will affect the measured ratios given by eqs. 1 through 3 and therefore the calculated refractive index. Optical component imperfections will be discussed in detail in a following section, but preliminary experiments<sup>3</sup> indicate that residual strain birefringence in the modulator is a major source of error.

With these considerations, data taken in February 1975 on the refractive index of polycrystalline ZnSe at  $10.6 \mu\text{m}$  as a function of incident angle are presented in Table 7. At angles greater than the Brewster angle,  $\theta_B$  ( $67.45^\circ$ ), the error increases to greater than 10%.

Several feedback systems have been built (Fig. 11) and are being tested to solve the stability problems. A variable gain (VGA) amplifier designed to go after the current-to-voltage preamplifier on the detector (Fig. 11) will compensate for any variation in source intensity. An alternative approach is a feedback loop to the laser itself via the PZT driven rear mirror (actually a grating) to keep the laser tube tuned to a constant output intensity. Three approaches to the problem of the modulator stability are being considered: (1) feedback of an acoustic signal picked up by a microphone attached to the mounting of the PEM, (2) feedback of an optical signal from a GaAs LED/silicon detector mounted to look through the edge of the ZnSe PEM (illustrated in Fig. 11), and (3) mounting of the entire PEM in a temperature control

---

<sup>3</sup>Ibid.

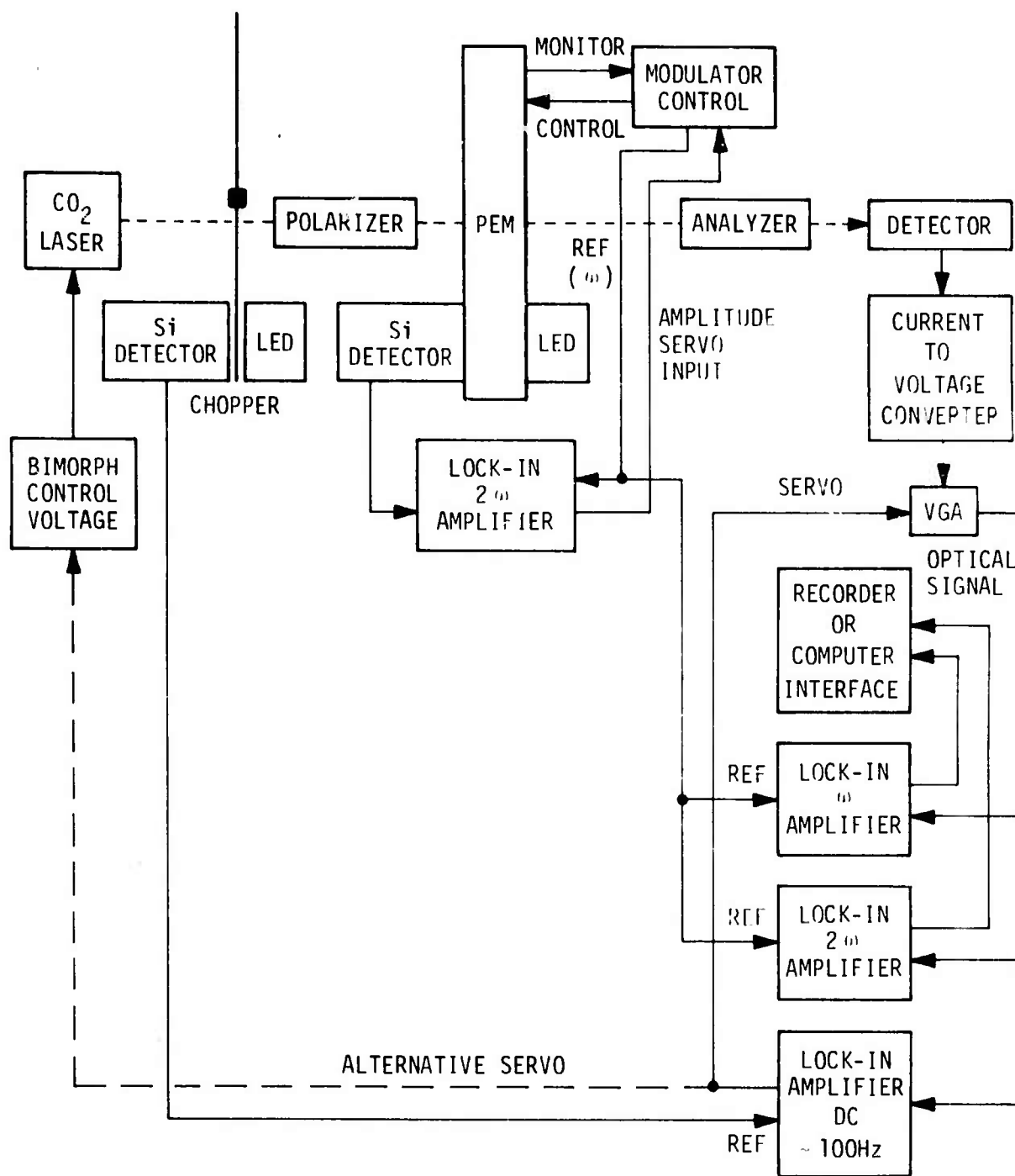


Fig. 11. Schematic of electronic components-infrared modulated light ellipsometer.

oven. The acoustic feedback approach achieves short term stability (several minutes average) but is subject to sudden jumps and will be affected by the temperature and relative humidity of the air layer between the PEM and the microphone. The optical feedback system shows the most promise now and is in the process of being tested.

### 3. Error Analysis

The following sources of systematic errors have been considered which involve imperfections in the optical components: residual strain and therefore birefringence in the polarizers and PEM, angular misalignment of the polarizers and PEM, linear polarization dichroism in the detector, and finite extinction ratio of the polarizers. The latter two problems can be either explicitly corrected for, as in the case of the extinction ratio of the polarizers, or minimized by arranging the optical system such that the detector sees only one polarization. Annealing procedures have been instituted to reduce the

TABLE 7. Refractive Index of ZnSe<sup>(a)</sup>

$\theta$	$\psi$ Experimental	$\psi$ Theoretical	$n_{\text{exp}}$
45°	26.46	27.92	2.224
50°	21.54	23.20	2.239
55°	16.80	17.67	2.331
60°	11.11	11.27	2.395
65°	4.42	3.94	2.444
67.45°	0.43	0	2.440

$n_{10.6 \mu\text{m}} = 2.403$  (ZnSe Single Crystal<sup>4</sup>).  
 (a) Raytheon Research Division, Waltham, MA 02154.

T1753

<sup>4</sup>A. Feldman, I. H. Malitson, D. Horowitz, R. M. Waxler, and M. J. Dodge, "Optical Properties of Polycrystalline Zinc Selenide," Proceedings of the Fourth Annual Conference on Infrared Laser Window Materials, 1974.

residual strain in the ZnSe components. The ZnSe pieces are heated to 425°C in an evacuated glass tube and allowed to cool slowly (12 hours or longer) to room temperature. Significant reduction of strain has been measured for ZnSe annealed by this procedure.

The effect of the remaining birefringence in the polarizers and modulator can be calculated and a computer program has been developed which simulates the ellipsometer including the alignment and residual birefringence errors. The Jones matrices representing the effect of the static strain birefringence in the polarizers are straightforward, but the PEM presents a different problem since it has both a static and a dynamic strain birefringence.<sup>5</sup>

It can be shown that for normal incidence the applicable Jones matrix  $\tilde{M}$  satisfies the differential equation

$$\frac{d \tilde{M}(z)}{dz} = -i \tilde{A}(z) \tilde{M}(z) \quad (6)$$

where  $\tilde{A}$  is given by

$$\tilde{A}(z) = \begin{pmatrix} \sin^2 \theta_B \frac{d\alpha_B}{dz} & -\sin \theta_B \cos \theta_B \frac{d\alpha_B}{dz} \\ -\sin \theta_B \cos \theta_B \frac{d\alpha_B}{dz} & \frac{d\alpha_m}{dz} + \cos^2 \theta_B \frac{d\alpha_B}{dz} \end{pmatrix}. \quad (7)$$

The coordinate  $z$  is measured along the path of the light from the point of entry into the modulator,  $\theta_B$  and  $\alpha_B$  are the angle and the amplitude of the static strain birefringence at  $z$ , and the dynamic strain  $\alpha_m = \alpha_m^0 \sin[\omega_m t]$ . The dynamic strain has been assumed to be applied in the  $x$ -direction (Fig. 12).

<sup>5</sup>J. C. Cheng, L. A. Nafie, S. D. Allen, and A. I. Braunstein, "Infrared Photoelastic Modulators," to be published.

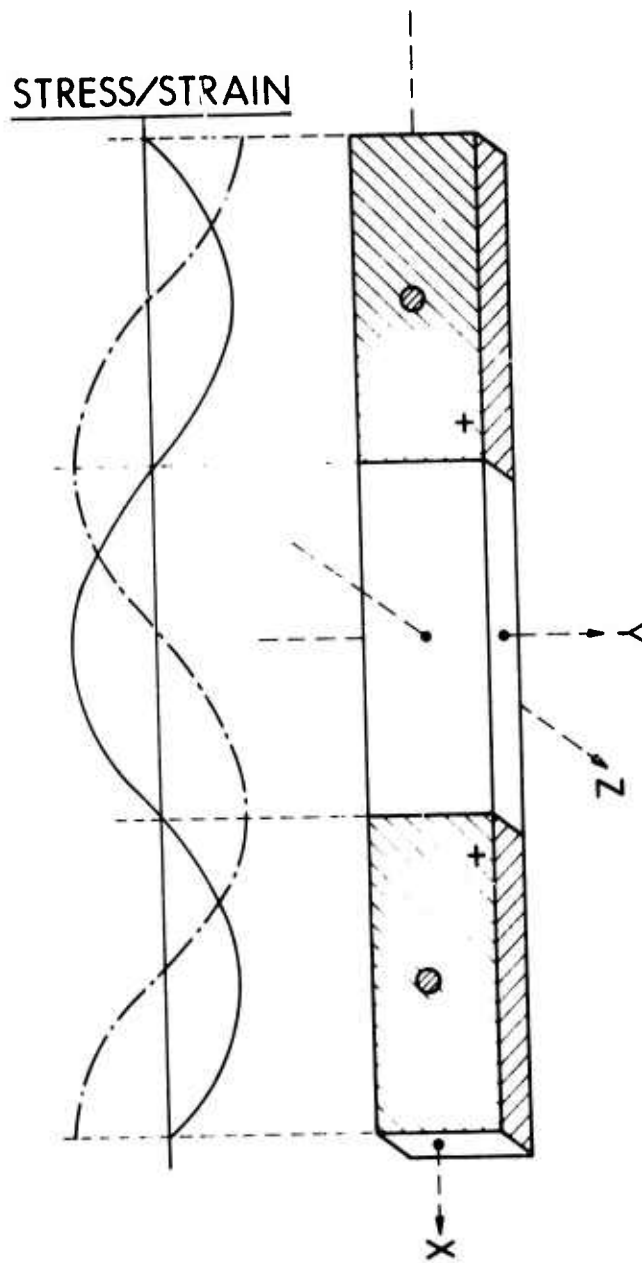


Fig. 12. The three-component photoelastic modulator. The + signs on the transducers denote the electrical polarization of the piezo electric drivers. The stress (solid line) and strain (broken line) are shown as a function of the position along the bar.

Equation (6) can be solved for  $\tilde{M}(L)$ , the Jones matrix which represents the light emerging from the modulator, under the assumption that  $\theta_B$  and  $\alpha_B$  are constant throughout the modulator. The solution is a matrix whose elements depend on  $\theta_B$ ,  $\alpha_B$ , and  $\alpha_m$  in a complicated way because of the coexistence of the static and dynamic birefringence effects throughout the optical path in the modulator.

For most practical cases the condition

$$\alpha_m^0 \gg \alpha_B \quad (8)$$

holds and then  $\tilde{M}(L)$  is given by

$$\tilde{M}(L) = \begin{pmatrix} 1 & 0 \\ 0 & e^{-i(\alpha_m + \alpha_B \cos 2\theta_B)} \end{pmatrix} \quad (9)$$

for most of the modulator drive cycle. Equation (9) has a simple physical interpretation. It is the matrix that would be obtained for a perfect modulator either preceded or followed by a birefringent plate whose axes are aligned with those of the modulator. Note that the most effective static birefringence is one that is, in fact, aligned with the modulator axes. For  $\theta_B = 45^\circ$  there is no effect. This is physically correct since the x and y components of the light passing through the modulator experience the same retardation for  $\theta_B = 45^\circ$  and only differences of retardation are observable.

For periods during the modulator cycle for which

$$\alpha_m \leq \alpha_B \quad , \quad (10)$$

the behavior is complicated. When  $\alpha_m$  passes through zero,  $\tilde{M}(L)$  reduces to the standard Jones matrix for a birefringent plate with maximum retardation  $\alpha_B$  at angle  $\theta_B$ . As  $\alpha_m$  increases, the solution approaches that are given in eq. (9). Thus, the principal axes of a

modulator with static birefringence display a periodic oscillation. However, for the magnitudes of  $\alpha_m^0$  and  $\alpha_B$  of interest to us, this phenomenon can be neglected, since it can be shown that  $\tilde{M}(L)$  departs significantly from the approximation of eq. (9) for only a small portion of each cycle. Therefore, we take  $M(L)$  to be

$$\tilde{M}(L) = \begin{pmatrix} 1 & 0 \\ 0 & e^{-i(\alpha_m^0 + \alpha_B^1)} \end{pmatrix} \quad (11)$$

with

$$\alpha_B^1 = \alpha_B \cos 2\theta_B \quad . \quad (12)$$

Data for which the predominant error is residual birefringence in the PEM can be corrected two ways: eq. (11) can be used to correct numerically for the static birefringence, or a birefringent plate with birefringence amplitude  $\alpha_B$  and at an angle  $\theta_B + 180^\circ$  could be placed in the optical train following the modulator to compensate for the residual birefringence. In practice, the birefringent amplitude of the compensator need only be small and the angle can be adjusted to achieve the same result. It is hoped, however, that such corrections will not be necessary if most of the residual strain can be removed by careful annealing and subsequent coating techniques.

Testing of the electronics package and improvement, if necessary, is of highest priority for the immediate future. After implementation of the stabilization schemes on the PEM amplitude and "DC," further tests of the residual strain and birefringence are planned with emphasis on carefully pinpointing the exact source of the major systematic errors. The computer simulation of the ellipsometer should be of great help in analyzing the systematic errors and correcting any data measured on films and substrates.

Replacement of the wire grid polarizers currently in use by some with higher extinction ratios on better quality annealed ZnSe is planned. Future plans include substitution of the laser source by a broad band light source and monochromator.

D. Damage Studies (C. R. Giuliano)

This task, devoted to laser-induced damage measurements in window materials, was begun in the latter three weeks of the reporting period. For this reason this section will not contain a description of experiment results, but instead will outline the status of our damage test capability for laser pulses at 10.6  $\mu\text{m}$  and briefly discuss the experimental plans for this task.

1. Objectives

The objectives of this task are to perform measurements of laser damage on window materials and coatings with the goal of determining the nature of the laser-induced failure mechanism. The results of the laser damage measurements will be combined with the results of other measurements performed on this program (e. g., absorption, surface finish, material growth parameters) to aid in the identification of the laser damage mechanism and to allow an assessment of the ultimate high-power laser performance capability of the materials of interest.

2. Accomplishments and Present Status

The present status of our laser damage test facility is one that is unique for CO<sub>2</sub> TEA lasers and reflects a substantial increase in flexibility over the capability previously described.<sup>6</sup> The present 10.6  $\mu\text{m}$  system yields pulsed laser output with the following parameters:

---

<sup>6</sup>"Laser Window Surface Finishing and Coating Technology," Final Report, AFCRL-TR-75-0041, January 1975.

- Variable focused spot sizes from 35  $\mu\text{m}$  diameter to 255  $\mu\text{m}$
- Continuously variable and reproducible energy output via rotatable wire grid polarizers
- Shot-to-shot energy monitoring
- Range of pulse durations from 0.6  $\mu\text{sec}$  to 6  $\mu\text{sec}$
- Control of pulse temporal profile from multi-longitudinal mode consisting of a train of partially mode locked pulses to single longitudinal mode consisting of a smooth temporal profile.

A description of the system as it currently stands is contained in the following pages. The main emphasis is placed on the recent innovations that have led to improved damage testing capability.

a. Description of Laser — The laser used to perform these damage threshold measurements has been refined for more than two years, and has been exclusively devoted to damage testing. For this study we used an ultraviolet preionized  $\text{CO}_2$  TEA laser developed at HRL, that yields up to 250 mJ at a pressure of 550 Torr from a 50 cm x 5 cm x 2.5 cm transverse discharge (Fig. 13). A separate pulse-forming network provides preionization through a row of resistively ballasted arcs on each side of the main discharge. The timing pulses for the preionizer and main discharges are generated in carefully shielded semiconductor timing circuits, with an adjustable delay, and amplified to a level sufficient to control the main switching tube. Both ignitron and thyatron switching tubes have been used (Figs. 14(a) and (b), respectively), with the latter proving slightly superior.

The discharge cavity is contained within a vacuum-tight Plexiglas cylinder 30 cm in diameter by 80 cm in length. Output Brewster windows with a 5 cm square aperture at each end permit external mounting of resonator optics.

M9555

4209-14

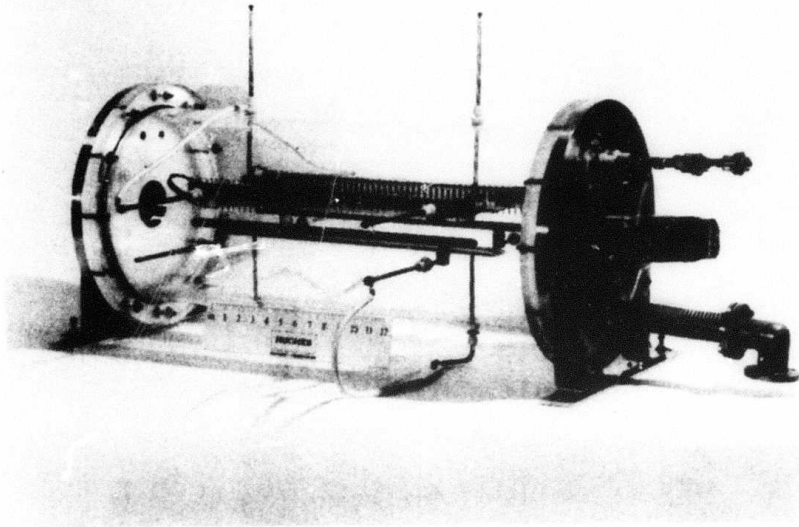


Fig. 13. View of transverse discharge section with uv preionizers.

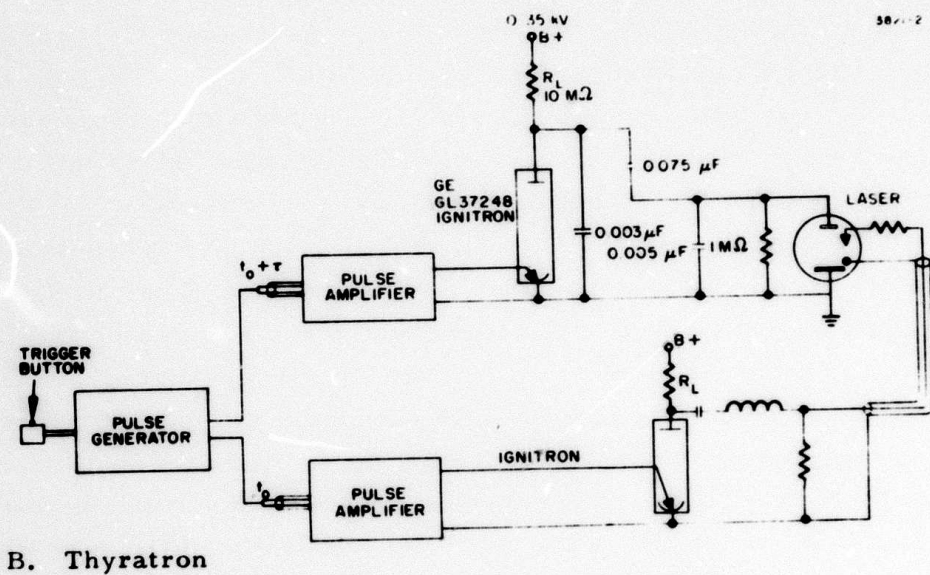
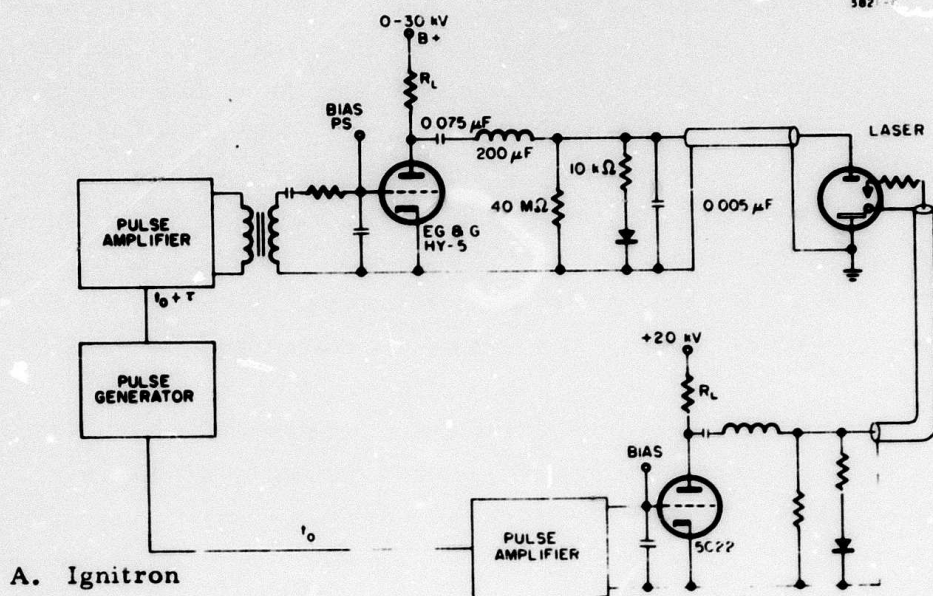


Fig. 14. Simplified schematic of double discharge electrical pulse forming network.

A gas handling system, illustrated in Fig. 15 permits a convenient choice between premixed gases or lower CO<sub>2</sub> fraction mixes used for long pulse operation. Operation up to atmospheric pressure is possible with any mixture, with or without a continuous flow of new gas. Since some breakdown of the CO<sub>2</sub> gas mix occurs from our electrical discharge, a continuous flow of new gas or about 3% H<sub>2</sub> is introduced into the mix to prevent arcing and erratic operation from contaminants. Operation with 3% H<sub>2</sub>, mixed by a fan within the sealed chamber, is more convenient. This mix is discarded at the end of each day.

Our optical cavity consists of a 2.5 m approximately hemiconfocal cavity with a 5 m metal reflector and an uncoated germanium resonant output reflector. An adjustable aperture set at about 1.2 cm selects the TEM<sub>00</sub> mode while providing an essentially untruncated output. The discharge chamber, optical cavity, sample chamber, and optical train are mounted upon a ferromagnetic honeycomb table for maximum stability (Fig. 16). The uncoated germanium etalon provides a convenient output coupler of 78% reflectivity which does not suffer from a cumulative laser damage with time that has been experienced with commercial coatings. Figure 17 is a schematic of the laser cavity, optical train, attenuators, and sample chamber.

The most satisfactory intracavity longitudinal mode selector was found to be a 1 m longitudinal discharge tube installed between the high pressure transverse discharge and the output coupler. This was operated at a pressure of approximately 20 Torr and discharge voltage of 12 kV by means of a separate power supply. This tube provided a single longitudinal mode smooth output with no mode heating evident, and also served to suppress the initial gain-switched spike characteristic of TEA lasers. It can also be operated as a cw CO<sub>2</sub> laser (using

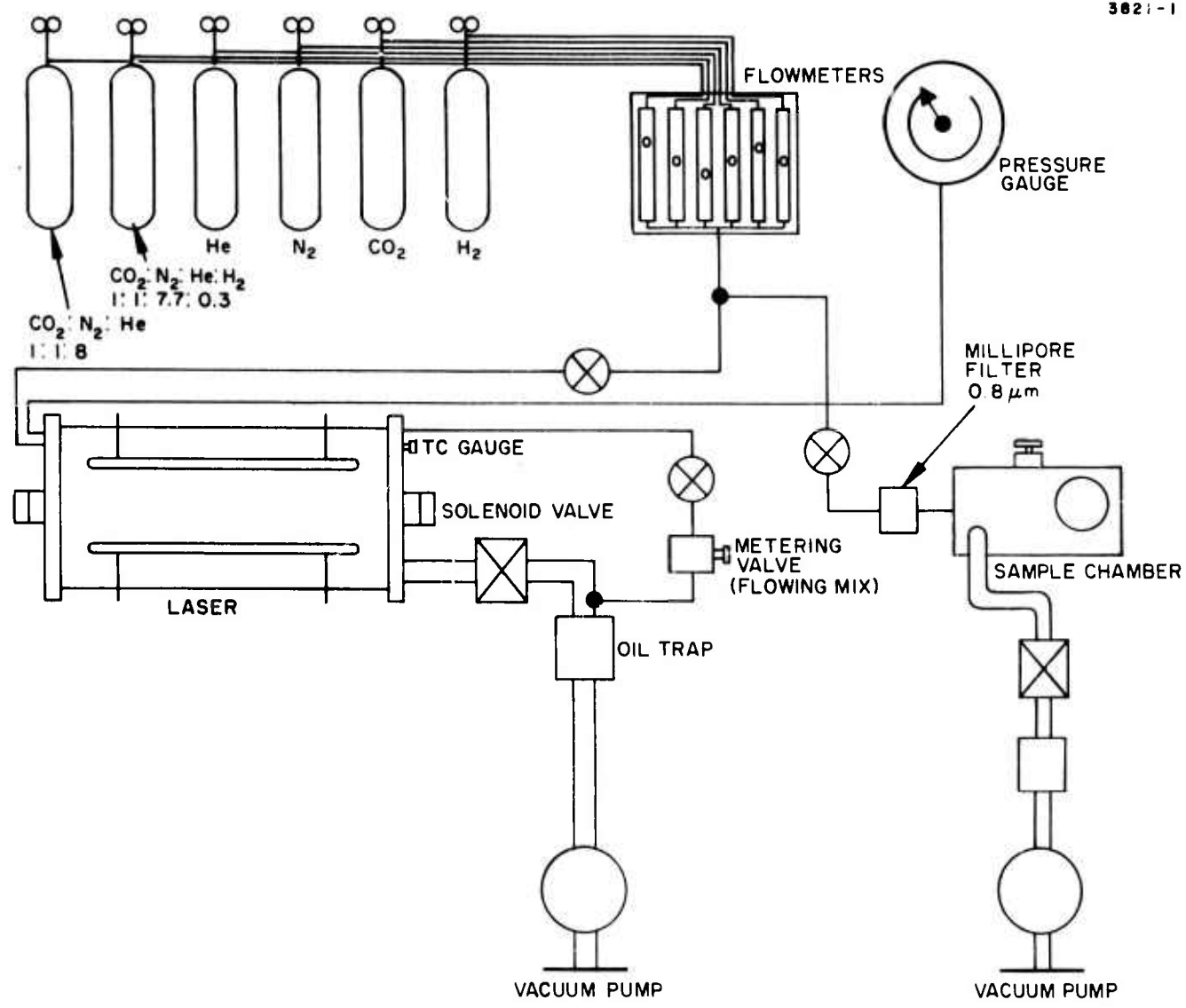


Fig. 15. Gas handling system for laser and sample chamber.

M11035

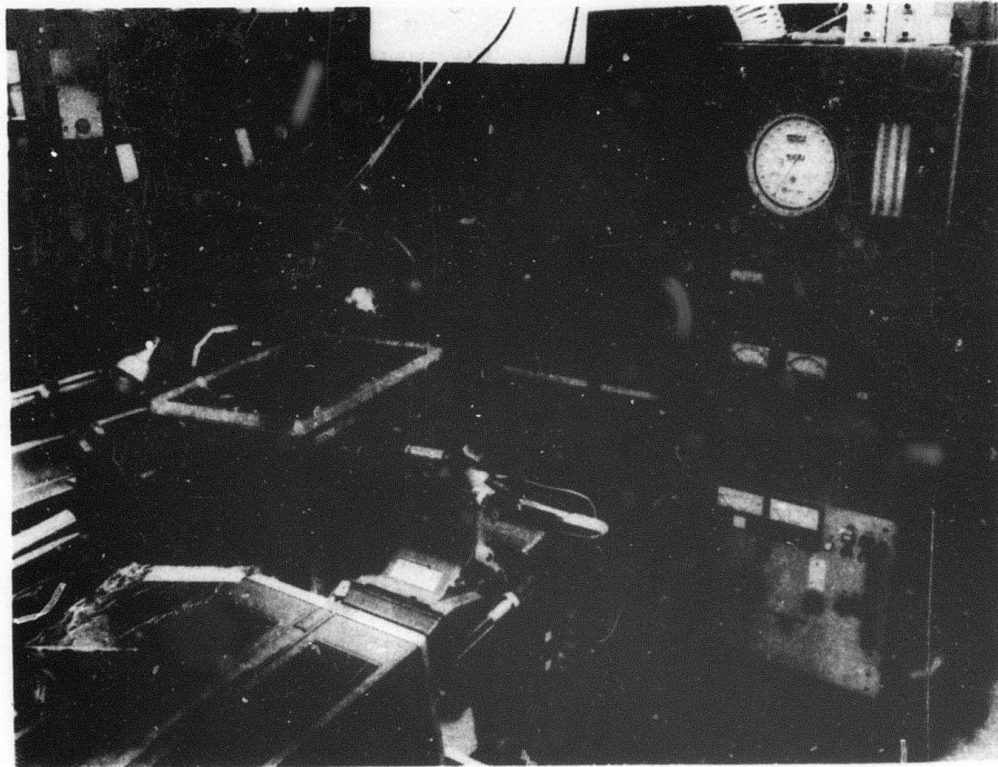


Fig. 16. Laser damage facility — gas handling system and power supplies to right, electrical pulse forming equipment is in background.

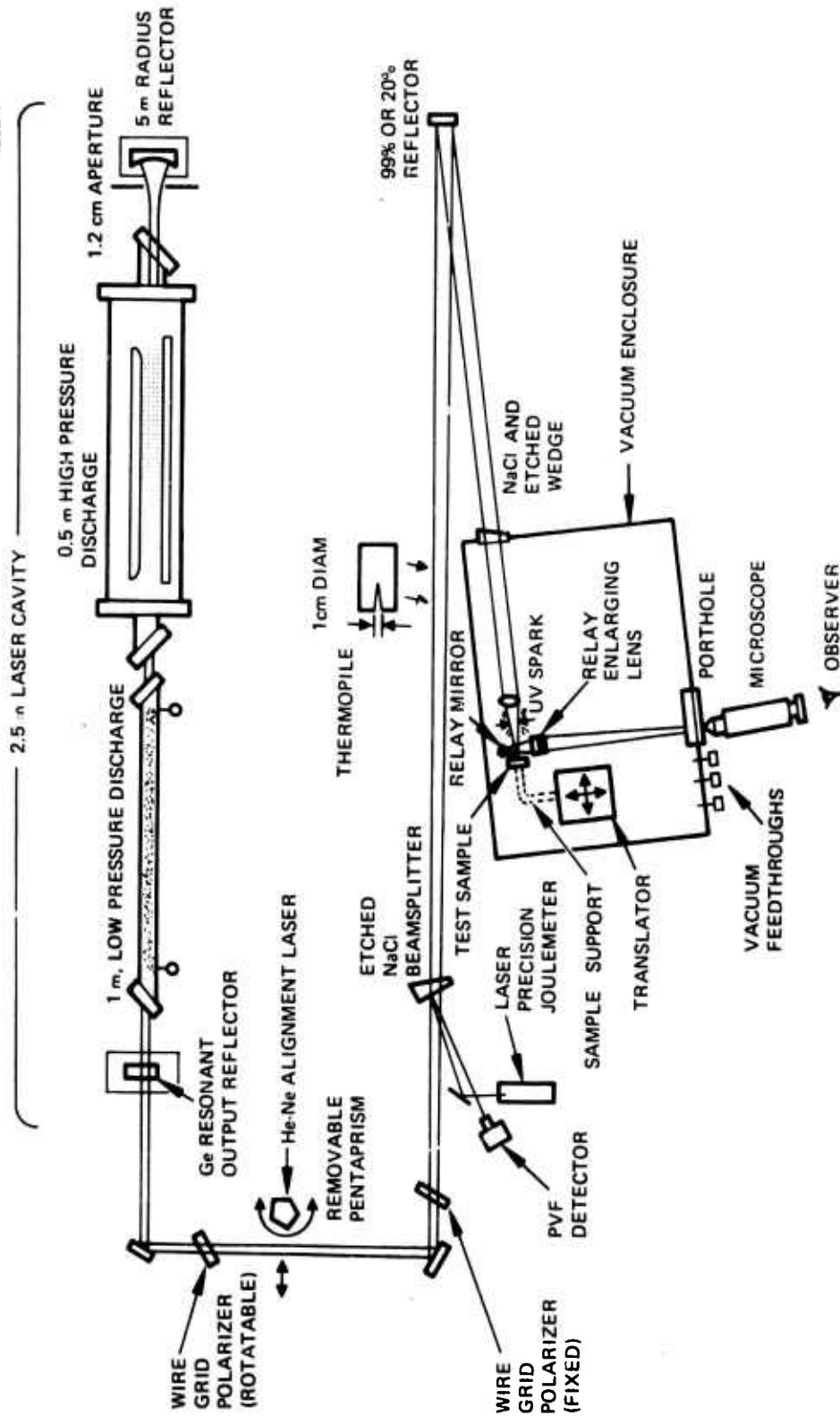


Fig. 17. Schematic of 10.6  $\mu\text{m}$  laser damage threshold apparatus, with relative disposition of laser, optical cavity, alignment train, attenuators, detectors, alignment system, and sample chamber with microscope and focusing lens.

the same resonator) providing an output beam coaxial with the pulsed output. When the low pressure tube is operated, a low level cw output of a couple of watts precedes the high power pulsed output by about 1 sec. About 175 mJ per pulse is available with this controlled mode of operation.

Reliability for thousands of shots, shot-to-shot reproducibility, good mode control, and the widest range of pulse length and energy consistent with the above, were the criteria which governed the development of this device.

b. Polarizers - Control of discharge voltage allows a little more than a 10 to 1 range of output energy, with a small change in temporal pulse shape toward the lower end of the discharge voltage range. (There has been no evidence of change in spatial profile with pump voltage.) Greater variations in intensity are desirable, since the damage resistance of the materials examined in this program can vary over several orders of magnitude. Two crossed polarizers provide a desirable way of continuously varying the output intensity without rotating the polarization. In conjunction with partially reflecting mirrors in the optical train, the use of polarizer attenuators has allowed us to study the effect of spot size on the damage threshold of a given material over a range of five to one.

Since birefringent materials for polarizers at  $10.6 \mu\text{m}$  are difficult to obtain, we can use wire grid polarizers or stacked plate polarizers. Hughes Research Laboratories and Caltech have developed a technique for making holographically-exposed sputter-etched wire grid polarizers and diffraction gratings suitable for high power usage. Utilizing our ZnSe finishing and AR coating technology a pair of  $2.5 \text{ cm}$  square polarizers on ZnSe were fabricated using gold wires of  $1 \mu\text{m}$  thickness with a  $1 \mu\text{m}$  space between wires. A molybdenum layer between the gold and the AR coating provides superior adhesion. A  $\text{ZnS } \lambda/2$  overcoat provides additional protection for the wire grid. These samples possessed individual extinction ratios about 50:1 and a combined transmission of about 80%.

c. Detectors - A Tektronix 7904 oscilloscope (EMI shielded) and fast camera provide a 500 MHz bandwidth system for use with a variety of pyroelectric and photon drag detectors. The most accurate measurements of pulse shape use a Rolfin germanium photon drag detector, which has better than 1 nsec risetime when used with a 50 $\Omega$  Tektronix 7A19 preamplifier. This detector is also calibrated in terms of megawatts per millivolt output. A low sensitivity that requires the entire laser output is the only disadvantage of this type of detector.

Alternately, a pyroelectric detector with differentiator has also been employed. To gain sensitivity a 100 MHz video amplifier system with differentiation has been satisfactory. With a well-shielded amplifier assembly and two-stage differentiation to improve electrical noise rejection, this system possesses sufficient sensitivity to utilize a 4% fraction of the beam.

A variety of energy monitors has been used to calibrate and monitor the laser output. The primary standard consists of a Hadron Model 100 thermopile which utilizes a double-cone principle. This is used to calibrate a pyroelectric energy monitor which intercepts 4% of the beam from a wedged NaCl beamsplitter. Several strontium barium niobate (SBN) detectors were tried for the application, but their long term tendency to depole made them unacceptable. A polyvinylfluoride (PVF) plastic film on a metal substrate has proved to be completely stable with time up to this point. This detector, supplied as a courtesy of O. M. Stafsudd, UCLA, is mounted in a well-shielded enclosure to suppress EMI and has a sensitivity of less than 0.5 mJ when used with an EMI shielded oscilloscope. A Laser Precision Joulemeter using a pyroelectric detector is being used as a secondary standard. This device has a 1 cm active area multiple bounce light trap type of detector and supplies a direct digital readout. At present, agreement with our calorimetric standard is satisfactory (~15%) at full laser output, but electrical noise pickup through the case appears to be limiting the accuracy of the device at lower pulse energy.

d. Calibration -- Determination of the absolute flux density in a beam has always remained the greatest difficulty in this type of research. Control of the beam spatial and temporal profile have made these aspects of this task reproducible, but no NBS standard is presently available for accurately measuring pulsed high power IR laser energy.

We have consistently attempted to improve the accuracy of our measurements by cross checking those calorimeters, thermopiles, and power meters used in this program. The Hadron Model 100 thermopile used as the primary standard in the damage portion of this program is believed to be our most accurate energy meter for the purpose and it also agrees quite well with other meters.

e. Sample Chamber -- An evacuated test chamber provides a controlled environment where testing can be conducted with a minimum of interference from the effects of dust, humidity, or air breakdown. In our previous studies at 10.6  $\mu\text{m}$  it was found that the presence of a surface in the focused beam greatly lowered the threshold for air breakdown. This breakdown could both obscure the true damage resistance of that surface, and affect the morphology of the damage.

The vacuum sample chamber is shown in Fig. 18. Its large size allows easy positioning of the sample with an x-y-z micrometer trans- later, which is operated through three vacuum feedthroughs, and its 12 portholes allow great flexibility in the type of experiment that can be performed. A spring loaded V-block accepts a variety of samples and an optical rail allows the use of a variety of focusing lenses. A spark electrode is provided above the sample to allow generation of the type of uv flux found in laser cavities. Finally, a 50x off-axis microscope system is incorporated into the sample chamber to allow close observa- tion of the sample during irradiation by the laser pulse. This is shown in detail in Fig. 19.

The laser beam enters the sample chamber through a wedges NaCl window and is focused by a germanium lens (Laser Optics, Inc.) mounted upon a separate stage. A mechanical pump with oil trap

M11037

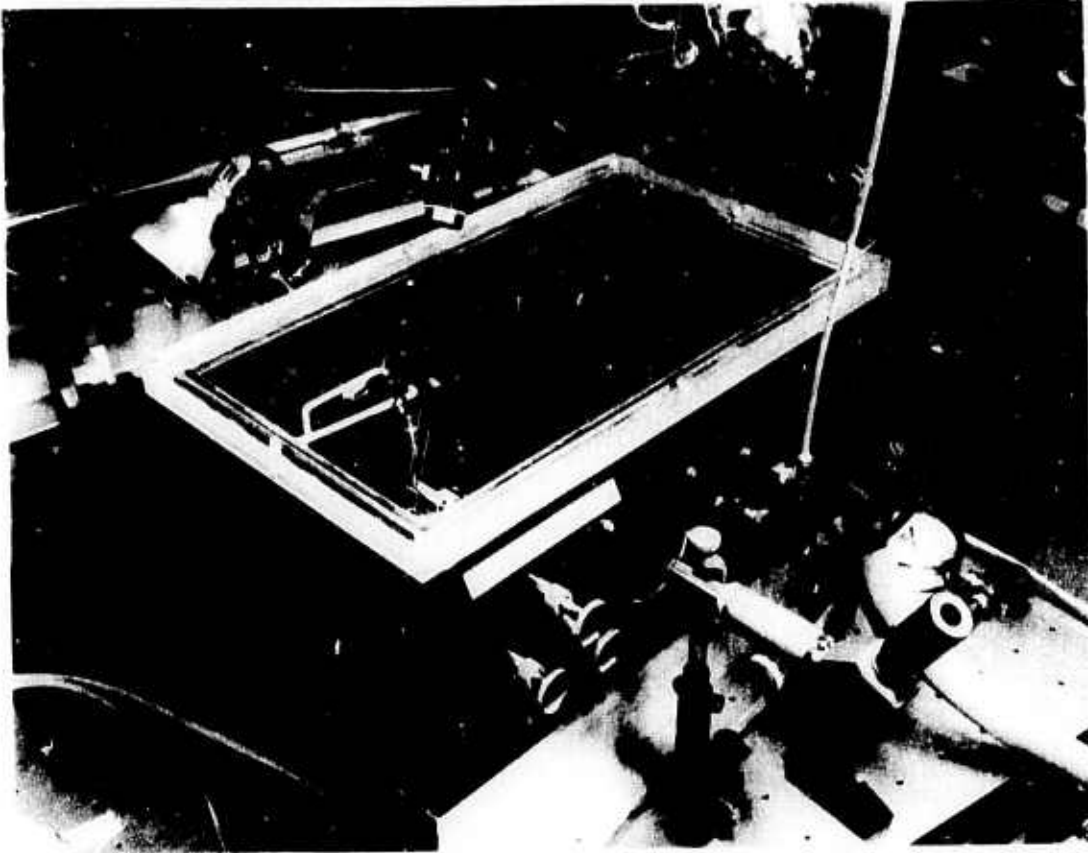


Fig. 18. Vacuum tight sample chamber with precision X, Y, Z translator, focusing lens, and microscope.

M11036



Fig. 19. Sample position in sample chamber showing focusing lens and off-axis microscope objective.

evacuates the chamber to about 100 mTorr, and bottled N<sub>2</sub> is passed through a 0.8 μm Millipore Corporation filter to refill the chamber, thus minimizing dust and other contaminants. Samples are kept in clean containers to minimize the necessity for cleaning the surfaces. Coatings receive only a dusting from a 0.8 μm filtered ionized dry nitrogen jet before testing.

f. External Diagnostics — It has been found that damage is not always accompanied by a visible plasma, and that the appearance of a plasma does not always indicate functional damage to the coating or substrate. To provide more resolution than possible within the sample chamber, several high resolution optical microscopes of up to 2000x are used to examine and photograph the samples after testing. Scanning electron microscope and x-ray microprobe devices have been available, although the type of damage mechanisms explored during this phase have not made this type of sophistication necessary.

g. Laser Performance — Continued improvement of 10.6 μm window materials and coatings has made greater flux densities increasingly desirable. This improvement has been achieved mostly by tighter focusing of the beam. An additional transverse discharge module has been available for those occasions where greater energy was desirable, but it has remained unnecessary in this program.

In addition to flux density, three laser parameters which are important to study are

- pulse duration
- pulse temporal shape
- spot size.

(1) Pulse Duration Control — In previous programs, the temporal envelope of the CO<sub>2</sub> laser output pulse used for damage studies has been the "typical" TEA laser pulse, i. e., a relatively short duration pulse consisting of a leading gain switched spike about 200 nsec

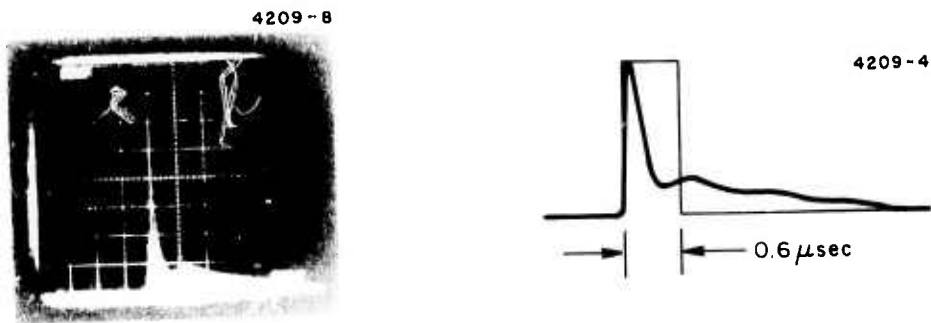
wide followed by a longer tail (Fig. 20(a)). The equivalent pulse duration of these short pulses is about 0.6  $\mu$ sec. (The equivalent pulse duration is defined as the width of the square pulse whose height is equal to that of the gain switched spike and whose total energy is equal to that of the laser pulse as shown in Fig. 20(b).)

A series of modifications was undertaken that was directed toward obtaining longer output pulses. The ability to utilize pulses of different duration for damage measurements is important for assessing the kinds of mechanisms that might be operative in the damage process. Furthermore, operational systems using e-beam discharge control might be expected to operate with 20  $\mu$ sec pulses, to optimize atmospheric propagation.

The approach that was taken utilized a combination of varying the laser gas mixture and total pressure and modifying the electrical pumping characteristics. The optimum energy available for the conventional short pulse requires a mixture of 55 Torr CO<sub>2</sub>, 55 Torr N<sub>2</sub>, 20 Torr H<sub>2</sub>, and 420 Torr He. The longer pulse requires 30 Torr CO<sub>2</sub>, 90 Torr N<sub>2</sub>, 20 Torr H<sub>2</sub>, and 310 Torr He. For the long pulse, the electrical pump pulse was stretched from 2  $\mu$ sec to the 8  $\mu$ sec pulse shown in Fig. 21.

At present it is possible to operate the laser with a long output pulse width of 6  $\mu$ sec FWHM, or an equivalent rectangular pulse width of 4  $\mu$ sec, having a total output energy comparable to that for short pulse operation. Figure 22 shows this long pulse laser output. (The equivalent pulse length allows direct comparison of peak power in different pulses by simply dividing energy density by equivalent pulse length.)

This technique employed to obtain long pulse operation proved superior to the method used previously, where a high reflectivity output coupler is used in combination with a very low CO<sub>2</sub> fraction and a short electrical pulse. Although the latter method is capable of pulses as long as 50  $\mu$ sec, the output energy was found to be unacceptably low when transverse mode control was incorporated.



a 0.6  $\mu$ sec.

b Short pulse.

Fig. 20. Equivalent pulse length.

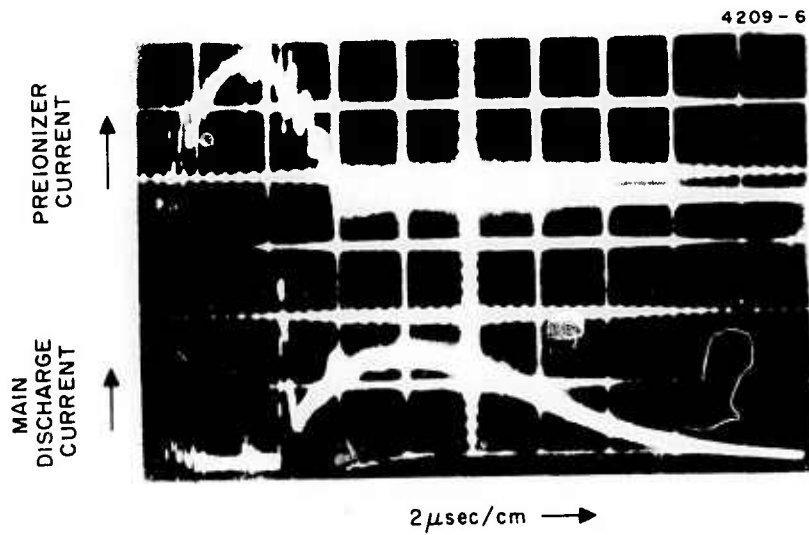
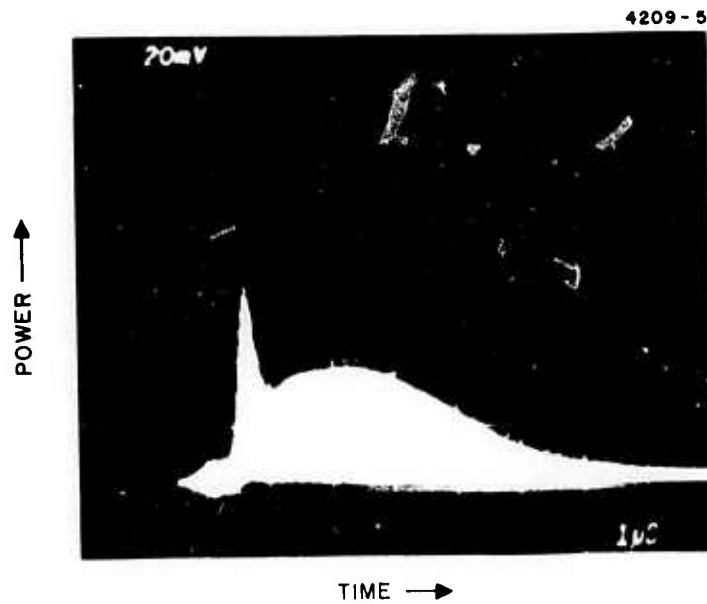
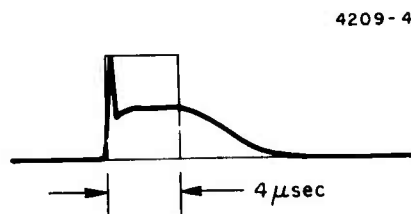


Fig. 21. Preionizer and main discharge current for long pulse operation.



(a) 4  $\mu$ sec



(b) Long pulse

Fig. 22. Equivalent pulse length.

(2) Longitudinal Mode Control - The CO<sub>2</sub> TEA laser facility normally operates in the lowest transverse mode and in several longitudinal modes. The result of this multilongitudinal mode operation is that the temporal output of the laser is modulated, i. e., it consists of a series of temporal spikes as shown in Fig. 23.

In fact, possibly due to the presence of the germanium resonant reflector within the cavity, the output tends to be mode locked. It has been considered desirable from the standpoint of achieving carefully controlled experimental conditions to operate the laser in a single longitudinal mode which would result in a temporally smooth output pulse. This kind of operation would allow more meaningful assignment of power densities to damage threshold measurements than has been possible to date with multilongitudinal mode operation.

Among the approaches taken toward the goal of achieving longitudinal mode control were the incorporation into the laser cavity of mode-selecting etalons, either in optical alignment with or tilted with respect to the cavity mirrors a gas cell containing SF<sub>6</sub> which is a saturable absorber at 10.6 μm (saturable absorbers act as longitudinal mode selectors when incorporated as intracavity elements) a number of variations of laser gas mix and pressure directed toward reducing the gain and gain bandwidth of the active medium the incorporation of a low pressure CO<sub>2</sub> discharge tube to act as an intracavity mode selector.

As mentioned previously, the last technique was chosen as the most desirable because it controlled both gain switching and mode heating. Some degradation of the transverse mode in the near field was observed from the presence of this tube, despite its diameter of about 2 cm. With careful alignment, this degradation was minimized, and because of the long propagation path, very little spatial modulation of the spot could be seen at the focusing lens. The measured spot sizes at the focus indicate that very little degradation of the focused spot has occurred, since the 10 in. f. l. and 5 in. f. l. lens still exhibited almost perfect diffraction limited performance.

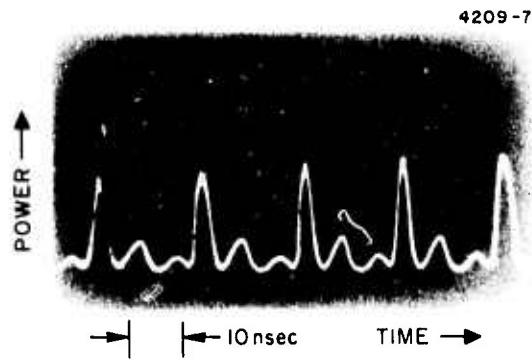


Fig. 23. Pulse slope measured with photon drag detector.

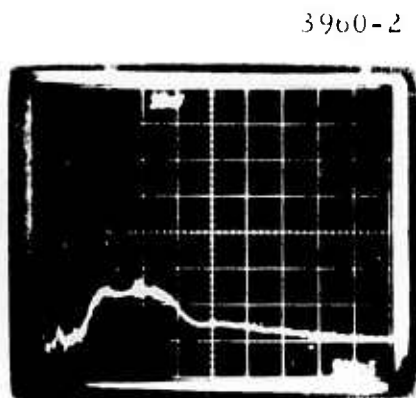


Fig. 24. Single longitudinal mode pulse of  $1 \mu\text{sec}$  duration.

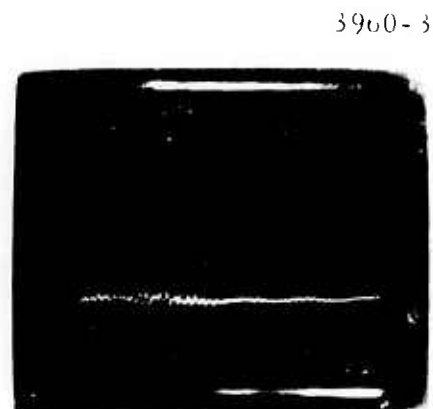


Fig. 25. 50 nsec/div expanded view of the main pulse (photon drag detector plus oscilloscope rise time  $\sim 1 \text{ nsec}$ ).

Figure 24 shows the temporal output pulse profile for the laser operating in the short pulse single longitudinal mode. The pulse is now very nearly rectangular and 1  $\mu$ sec in duration. Figure 25 is an expanded view of the pulse form taken at the top of the pulse, and it now shows a virtually flat-topped pulse with no modulation. Figure 26 shows a comparison between a multilongitudinal mode long pulse output, and the single-longitudinal mode long pulse output.

(3) Rotational Line Control — Some preliminary consideration has been given to monitoring which rotational line the laser is operating upon. With the output etalon used previously the laser was found on one occasion to be running on P16 with a grating spectrometer. Recently the low power cw output of the laser (without the TEA discharge) was measured with a homodyne detector system, and found to be operating on P18. It is presumed that the high power pulse is also at P18, since that frequency of oscillation has first been initiated by the cw oscillation.

h. Summary of Laser Performance — Control of a number of operating parameters of the laser has been necessary to achieve the present output, pulse length, and pulse shape. Table 8 illustrates many of the parameters that were varied in pursuit of better control of the laser output. Some relevant changes which improved those desirable aspects of the laser output include electrical pump pulse shape and duration, electrode profile and spacing, gas mixture and pressure (especially CO<sub>2</sub> fraction and the addition of H<sub>2</sub>), and a modest increase in mirror radius.

In its final form this system, for the first time, permits us to study the influence pulse length over approximately a ten to one range, to compare the effect of pulse modulation and the high instantaneous power in a gain-switched mode-locked pulse with a smooth single longitudinal mode pulse of easily characterized instantaneous intensity, and to compare the effect of beam spot size upon damage threshold over a range of five to one.

4209-22

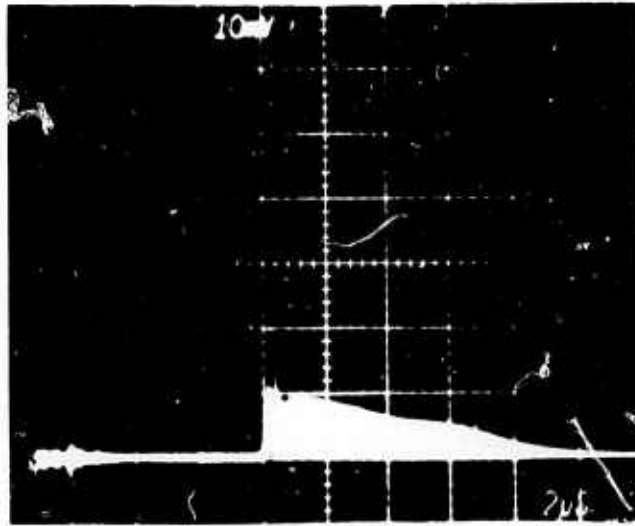


Fig. 26(a). 4  $\mu$ sec equivalent pulse length, modified.

4209-23

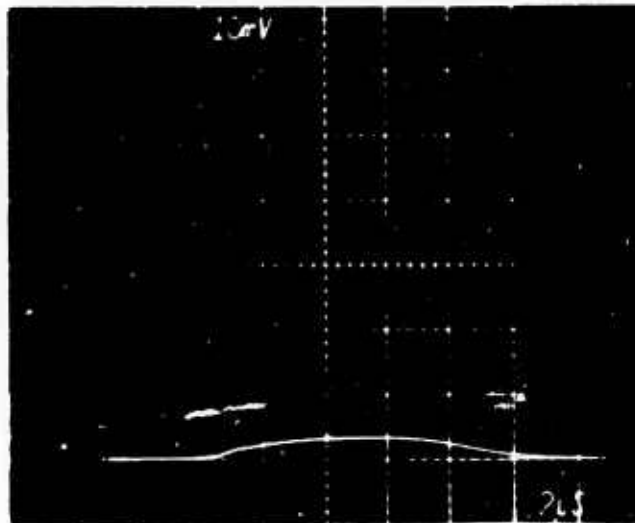


Fig. 26(b). 6  $\mu$ sec single longitudinal mode pulse.

TABLE 8. Laser Operating Parameters

Parameters	Operational Constraints					
	Energy Output	Laser Pulse Duration	Laser Pulse Temporal Profile	Glow-to-Arc Transition	Alignment Stability	Transverse Mode Size/Profile
Electrical						
Pump pulse shape	X		X			
Pump pulse duration	X		X			
Pump pulse energy	X					
Timing of pump pulse relative to preionizer pulse				X		
Electrode profile				X		X
Electrode spacing				X		X
Discharge volume	X					X
Discharge uniformity				X		
Gas mixture						
Relative composition (CO <sub>2</sub> , N <sub>2</sub> , He)	X					

TABLE 8. Laser Operating Parameters (Contd)

Parameters	Operational Constraints					Transverse Mode Size/ Profile
	Energy Output	Laser Pulse Duration	Laser Pulse Temporal Profile	Glow-to-Arc Transition	Alignment Stability	
Total pressure	X	X				
Optical cavity						
Mirror reflectivities (Cavity Q, output coupling fraction)	X	X				
Cavity length		X			X	X
Mirror curvatures	X				X	X

T1568

To our knowledge, this is the first time a single transverse mode CO<sub>2</sub> TEA laser has been available to study laser damage with a variable pulse length and single longitudinal mode control.

### 3. Future Plans

The plans for the immediate future are directed toward continued study of the damage of alkali halide window materials. Besides measurement of the damage thresholds for materials that have been grown by different techniques and that possess different degrees of material purity we plan to study the damage as a function of laser longitudinal mode control and pulse duration. One of the phenomenological studies to be performed is to monitor the temporal shape of the pulse transmitted through the sample using a photon drag detector / fast oscilloscope combination. This type of experiment will give statistics related to the time at which breakdown is seen to occur and will allow us to determine the extent to which peak power density is a factor in determining dielectric breakdown. A comparison of temporal shapes of transmitted pulses for partially mode locked operation to that for single longitudinal mode generation may afford some insight into the temporal dependence of so called "intrinsic" breakdown phenomena.

### III. SUMMARY

The work on thorium tetrafluoride ( $\text{ThF}_4$ ) film preparation under ultrahigh vacuum conditions which was reported in preliminary form in the Final Report, January 1975,<sup>6</sup> has been completed. The  $\text{ThF}_4$  films prepared exhibited absorption index values ( $k$ ) in a range of 0.7 to  $1.1 \times 10^{-3}$ . These values are the same as those we obtain using conventional high vacuum oil diffusion pumped systems. Since we do not find any benefit in using ultrahigh vacuum for  $\text{ThF}_4$  films preparation, we recommend that conventional high vacuum systems be used.

Surface finishing work for KCl emphasized examination of various liquid etchants to determine their compatibility with pitch laps used for surface polishing. Table 2 shows a list of the liquids tried and their effect on pitch. For those liquids which did not dissolve pitch to a great extent, etch rate studies on KCl surfaces were performed. Table 3 shows surface removal rates in  $\mu\text{m}/\text{min}$  for various liquids. Hard and soft pitch laps were used in attempts to maintain surface flatness and keep surface scratches at a minimum using triacetin as the polishing abrasive vehicle. Total sphericity (flatness of both sides) is held to 2 or 3 fringes in the visible and faces are parallel within 5 sec of arc.

The work on the modulated light ellipsometer continued. Data on the refractive index of polycrystalline ZnSe at  $10.6 \mu\text{m}$  as a function of incident angle is presented in Table 7. Various feedback control stabilization schemes are described to provide stability to the light source and the PEM used to obtain  $10.6 \mu\text{m}$  operation.

The present status of our laser damage test facility is unique for  $\text{CO}_2$  TEA lasers and reflects a substantial increase in flexibility over the capability described in Ref. 1. In particular, the range of pulse durations has been extended to cover from  $0.6 \mu\text{sec}$  to  $6 \mu\text{sec}$ , and control of pulse temporal profile from multilongitudinal mode consisting of a train of partially mode-locked pulses to single longitudinal mode consisting of a smooth temporal profile, has been achieved.

---

<sup>6</sup>Ibid.

Extensive consultation and ad-hoc reviews of the surface and coatings program were held with ARPA, NRL, NWC, AFWL, AFML, and AFCRL.

V. PRESENTATIONS

A paper was presented by S. D. Allen at the Conference on Optical Properties of Highly Transparent Solids, Waterville Valley, New Hampshire, February 1975, entitled "A 10.6 Micron Modulated Light Ellipsometer."

**Preceding page blank**